

# Colloidal Processing of Ceramics

Jennifer A. Lewis

Materials Science and Engineering Department, University of Illinois at Urbana-Champaign, Urbana, Illinois 61801

**Colloidal processing of ceramics is reviewed with an emphasis on interparticle forces, suspension rheology, consolidation techniques, and drying behavior. Particular attention is given to the scientific concepts that underpin the fabrication of particulate-derived ceramic components. The complex interplay between suspension stability and its structural evolution during colloidal processing is highlighted.**

## I. Introduction

THE term “colloid” is used to describe particles that possess at least one dimension in the size range  $10^{-3}$ – $1\ \mu\text{m}$ . A distinguishing feature of all colloidal systems is that the contact area between particles and the dispersing medium is large. As a result, interparticle (or surface) forces strongly influence suspension behavior. The study of colloidal phenomena, known as colloid science, has led to technological advances in numerous areas, including ceramic processing, coatings, paints, inks, drug delivery, and even food processing.

Colloidal processing offers the potential to reliably produce ceramic films and bulk forms through careful control of initial suspension “structure” and its evolution during fabrication.<sup>1–3</sup> This approach involves five basic steps: (1) powder synthesis, (2) suspension preparation, (3) consolidation into the desired component shape, (4) removal of the solvent phase, and (5) densification to produce the final microstructure required for optimal performance. Unintentional heterogeneities (or defects) introduced in any stage of the fabrication process persist or become exacerbated during densification.<sup>1</sup> Hence, there is a continual drive toward improved understanding of colloidal stability and assembly to achieve the desired spatial distribution of phases (including porosity) in as-consolidated bodies.

The purpose of this paper is to review colloidal processing of ceramics, including related areas of colloid science. Particular emphasis is given to advances made in recent decades. In Section II, we provide a historical perspective from ancient crafting to emerging approaches. In Section III, we outline the various types of interparticle forces, including van der Waals, electrostatic, steric, and depletion forces, that govern colloidal stability in the

absence and presence of processing additives. In Section IV, we discuss the impact of colloidal stability and compositional effects on the rheological behavior of ceramic dispersions. In Section V, we present an overview of conventional and emerging consolidation techniques used to fabricate ceramic components. In Section VI, we examine the drying behavior of as-consolidated bodies. In Section VII, we offer a perspective on the future direction of colloidal processing. Our principal purpose is to elucidate the structure–property evolution that occurs during colloidal processing before component densification at elevated temperatures. The latter topic is beyond the scope of this review. The interested reader is referred to the review by Lange,<sup>1</sup> which provides an excellent description of microstructural evolution during densification and its dependence on powder processing.

## II. Historical Perspective

Ceramics have been processed by colloidal routes for several millennia. The ancient crafts principally involved clay-based ceramics, with the earliest developments dating back to hand-formed pottery in 7000 BC and hand-thrown pottery in 3500 BC.<sup>4,5</sup> Many of the traditional forming methods used today, including slip casting, extrusion, filter pressing, and dry pressing, originated in the 1700s and 1800s.<sup>5,6</sup> In the early 1900s, research activities focused on understanding the behavior of clay-based systems and characterizing ceramic crystal structures.

Colloidal processing of ceramics has emerged only recently as a scientific field of research. The pioneering work of ceramists,<sup>2,7–10</sup> who first demonstrated the important relations between structure, properties, and processing of ceramics; of researchers,<sup>11–14</sup> who developed novel synthetic pathways for producing ceramic powders with controlled purity, morphology, and size; and of colloid scientists, who developed the theoretical framework for modeling colloidal interactions in suspension<sup>15–20</sup> as well as techniques for directly measuring such forces,<sup>21–24</sup> have provided the scientific foundations of this field. Indeed, it is the interplay between these groups of researchers and the collective body of knowledge generated that has led to the significant advances outlined in the remainder of this review.

The clay–water system, the first colloidal system to be studied extensively, is featured prominently in several ceramics texts.<sup>4,5,25</sup> This system serves as a basis for many traditional ceramics. Clay particles have a platelike morphology commonly consisting of negatively charged faces and positively charged edges when suspended in a polar solvent, such as water. These particles readily undergo cation exchange reactions, swelling, adsorption, and even intercalation of organic species to alter their surface charge,

V. A. Hackley—contributing editor

Manuscript No. 188788. Received January 24, 2000; approved June 20, 2000.  
\*Member, American Ceramic Society.

chemistry, and crystal structure.<sup>25</sup> Processing of clay-based ceramics is aided by their inherently plastic nature, which provides excellent shape-forming capabilities. The plasticity of clay suspensions results in part from their tendency to form the “house of cards” structure shown in Fig. 1. This aggregated particle network results in an appreciable yield stress (refer to Section IV) that allows component shape to be maintained after the applied forming pressure is removed. Aqueous clay suspensions continue to serve as an archetype for our field.

Unlike clay-based systems, plastic systems must be engineered for ceramic suspensions that serve as feedstock for advanced ceramic components. This can be accomplished by incorporating organic processing additives, such as polymers and plasticizers. These species serve to modify rheological behavior and impart handling strength to as-formed ceramic bodies. Their presence, however, poses significant challenges, especially for components of large dimension and/or high binder loading. For example, undissolved organic species<sup>26</sup> or uncontrolled decomposition reactions<sup>27</sup> generate defects during binder removal. Moreover, the debinding times required for complex parts, such as injection-molded engine components, are typically long, on the order of several days.<sup>27–29</sup>

Two decades ago, Bowen and co-workers<sup>8,13</sup> proposed that binder-free, monodisperse colloidal suspensions were optimal for achieving the microstructural homogeneity required for functional ceramics. Unfortunately, these systems lacked the desired plasticity mentioned above. Furthermore, they did not yield ceramic bodies with a monomodal pore-size distribution, even when crystallization occurred during consolidation.<sup>2,30</sup> Despite these limitations, monodisperse colloidal systems (e.g., those based on silica spheres)<sup>11</sup> have served as excellent model systems for the study of aggregation,<sup>31–35</sup> rheological,<sup>36–40</sup> sedimentation,<sup>40–42</sup> and drying phenomena<sup>3,43</sup>

Lange and co-workers<sup>44,45</sup> proposed a new paradigm for powder processing in the early 1990s. Their approach embodied many principles that guided earlier efforts, including use of powders with controlled size, morphology, and purity; no added binder; and dispersion control.<sup>8</sup> However, their purpose was to induce a “claylike” response by tailoring interparticle forces in suspension. Specifically, the colloidal system of interest was first prepared in the dispersed (stable) state to effectively eliminate powder agglomerates—an important source of unwanted defects—via milling, sedimentation, and/or filtration processes. The system was then adjusted to a weakly flocculated state (refer to Section III) to create the desired plasticity needed for forming as well as to minimize mass and/or phase segregation during storage and handling.

Several forming methods have been developed, such as direct coagulation casting<sup>46,47</sup> and gel casting,<sup>48–50</sup> which rely on transforming ceramic suspensions from the dispersed to the gelled state (refer to Section V). Such methods allow near-net-shaped ceramics to be formed with tailored rheological properties, minimal organic binder content, good handling strength, and excellent microstructural homogeneity. The as-consolidated bodies contain a gelled network of colloidal particles<sup>46,47</sup> or organic species.<sup>48–50</sup>

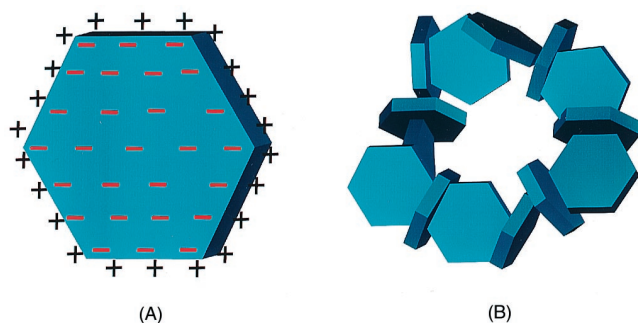


**Fig. 1.** Schematic illustration of clay particles suspended in water: (A) individual particle and (B) aggregated particle network formed because of the attraction between oppositely charged faces and edges.

Solid freeform fabrication (SFF) of ceramics is a novel method for producing complex components with locally controlled composition and structure. Several SFF techniques have been developed, including three-dimensional printing (3DP),<sup>51</sup> robocasting,<sup>52</sup> stereolithography,<sup>53</sup> computer-aided manufacturing of laminated engineering materials (CAM-LEM),<sup>54</sup> and fused deposition.<sup>55</sup> Some routes<sup>51,52</sup> rely on the colloidal approach to produce feedstock with the desired rheological and consolidation behavior, while others<sup>53–55</sup> require high organic loading. Although originally developed for rapid prototyping, SFF techniques offer potential for forming specialized ceramic components.

### III. Interparticle Forces

Through careful control of interparticle forces, colloidal suspensions can be prepared in the dispersed, weakly flocculated, or strongly flocculated states, as shown schematically in Fig. 2. In the dispersed state, discrete particles that exist in the suspension repel one another on close approach, provided the repulsive barrier is  $\gg k_bT$ . In the weakly flocculated state, particles aggregate in a shallow secondary minimum (well depth  $\approx 2\text{--}20 k_bT$ ), forming isolated clusters (or flocs) in suspension at volume fractions below the gel point ( $\phi < \phi_{\text{gel}}$ ) or a particle network at higher volume fractions ( $\phi \geq \phi_{\text{gel}}$ ). In this case, an equilibrium separation distance exists between aggregated particles. In contrast, particles aggregate into a deep primary minimum in the strongly flocculated (or coagulated) state, forming either a touching particle network or individual clusters in suspension, depending on their concentration.

Colloidal stability is governed by the total interparticle potential energy,  $V_{\text{total}}$ , which can be expressed as

$$V_{\text{total}} = V_{\text{vdW}} + V_{\text{elect}} + V_{\text{steric}} + V_{\text{structural}} \quad (1)$$

where  $V_{\text{vdW}}$  is the attractive potential energy due to long-range van der Waals interactions between particles,  $V_{\text{elect}}$  the repulsive potential energy resulting from electrostatic interactions between like-charged particle surfaces,  $V_{\text{steric}}$  the repulsive potential energy

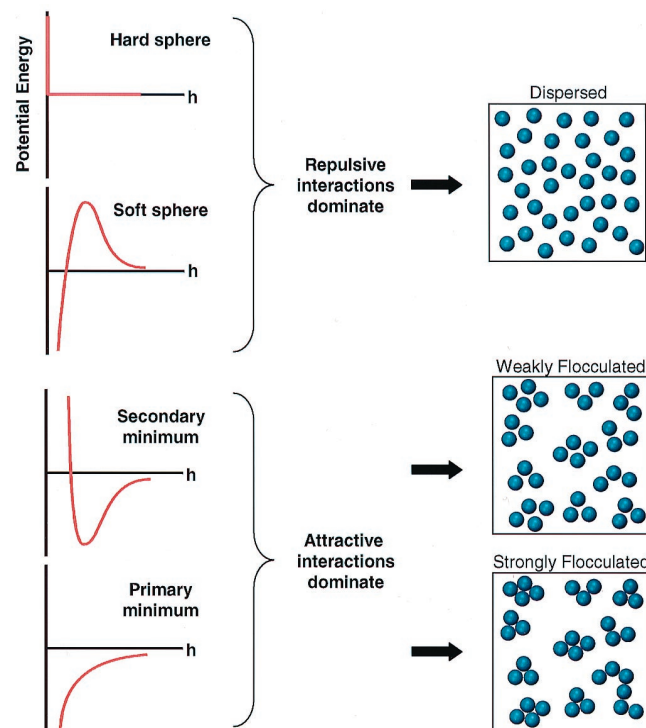


**Fig. 2.** Schematic illustration of the relationship between the total interparticle potential energy and the resulting suspension structure. (Ordinate axis is generally scaled to  $kT$ ; i.e., energy resulting from thermal fluctuations.)

## Glossary of Terms

$a$	particle radius	$V_{\text{total}}$	total interparticle potential energy
$a_{\text{dep}}$	depletant radius	$V_{\text{vdW}}$	van der Waals potential energy between particles
$A$	Hamaker constant	$\bar{V}$	molar volume of colloidal phase
$A(h)$	Hamaker function	$W$	stability ratio
$A_s$	specific surface area	$z$	position
$b$	proportionality constant	$z_i$	valence of ions of type $i$ in solution
$D$	permeability	$\alpha$	fraction of ionizable groups along polyelectrolyte chain
$E$	applied electric field	$\delta$	adsorbed layer thickness
$f_H$	Henry constant	$\partial$	phase angle
$F$	Faraday constant	$\Delta\rho$	density difference between colloidal particles and suspending medium
$g$	gravitational constant	$\Delta P$	pressure drop
$G'$	dynamic storage modulus	$\epsilon_0$	permittivity of free space
$G''$	dynamic loss modulus	$\epsilon_r$	relative dielectric constant
$G^*$	complex shear modulus	$\eta$	apparent viscosity
$G'_d$	dimensionless dynamic storage modulus	$\eta_{\text{equil}}$	plateau apparent viscosity
$G''_d$	dimensionless dynamic loss modulus	$\eta_o$	solution viscosity
$G'_{\text{equil}}$	plateau dynamic storage modulus	$\eta_{\text{rel}}$	relative viscosity
$h$	minimum separation distance between particle surfaces	$\dot{\gamma}$	shear rate
$H$	layer thickness	$\gamma_{\text{LV}}$	surface tension of liquid–vapor interface
$H_{\text{eq}}$	equilibrium height	$\Gamma_{\text{ads}}$	mass of adsorbed species per solid surface area
$J$	liquid flux	$\kappa^{-1}$	Debye–Huckel screening length
$k$	rate constant for flocculation of given colloidal system	$\Psi_0$	surface potential
$k_b$	Boltzmann constant	$\mu_0$	chemical potential of solvent
$k_0$	rate constant for fast, irreversible flocculation	$\mu_{\text{poly}}$	chemical potential of polymer solution
$K$	hydrodynamic shape factor	$\nu$	Poisson's ratio
$l_{\text{cap}}$	length scale for capillary migration of liquid	$\phi$	volume fraction of colloidal particles in suspension
$m$	power-law exponent	$\phi_2^a$	average volume fraction of segments in adsorbed layer
$M_{a(2)}$	molecular weight of adsorbed species	$\phi_{\text{dep}}$	volume fraction of depletant species in solution
$n$	power-law exponent	$\phi_{\text{eff}}$	effective volume fraction of colloidal particles in suspension
$N$	number density of colloidal particles in suspension	$\phi_{\text{gel}}$	volume fraction of colloidal particles in suspension at the gel point
$N_i$	number density of ions of type $i$ in solution	$\phi_{\text{max}}$	maximum volume fraction of colloidal particles in suspension
$P_{\text{cap}}$	capillary pressure	$\Phi(z)$	local volume fraction of solids at position $z$
$P_y$	compressive yield stress	$\Pi$	osmotic pressure
$Pe$	Peclet number	$\Pi_{\text{poly}}$	osmotic pressure of polymer solution
$P(z)$	applied stress at position $z$	$\rho$	density of solution
$r_h$	hydraulic radius	$\rho_2$	density of adsorbed species
$r_p$	characteristic pore radius	$\rho_s$	density of colloidal particles
$R$	gas constant	$\sigma_o$	plane of charge
$Re$	Reynold's number	$\sigma_{\text{decay}}$	decay stress measured during drying
$t$	time	$\sigma_{\text{max}}$	maximum stress measured during drying
$T$	temperature	$\sigma_{\text{rise}}$	rise stress measured during drying
$T_{\text{gel}}$	gel temperature	$\sigma_{\text{residual}}$	residual drying stress
$U_0$	terminal settling velocity	$\sigma_s$	compressive stress imposed on particle network during drying
$v_1$	molar volume of solvent	$\tau$	shear stress
$V_{\text{dep}}$	depletion potential energy between particles resulting from nonadsorbed species	$\tau_y$	shear yield stress
$V_e$	evaporation rate	$\omega$	frequency
$V_{\text{elect}}$	electrostatic potential energy between charged particles	$\omega_d$	dimensionless frequency
$V_m$	molar volume of solvent	$\chi$	Flory–Huggins parameter
$V_{\text{max}}$	maximum repulsive barrier height	$\zeta$	zeta potential
$V_{\text{min}}$	depth of secondary minimum		
$V_{\text{steric}}$	steric potential energy between particles resulting from adsorbed species		
$V_{\text{structural}}$	structural potential energy between particles resulting from nonadsorbed species		

resulting from steric interactions between particle surfaces coated with adsorbed polymeric species, and  $V_{\text{structural}}$  the potential energy resulting from the presence of nonadsorbed species in solution that may either increase or decrease suspension stability. The first two terms of Eq. (1) constitute the well-known DLVO theory developed by Derjaguin and Landau<sup>16</sup> and Verwey and Overbeek.<sup>17</sup> This theory, which predicts the stability of colloidal

particles suspended in polar liquids, is a cornerstone of modern colloid science.

**(1) van der Waals Forces**

Long-range forces resulting from van der Waals (vdW) interactions are ubiquitous and always attractive between like particles.

$V_{\text{vdW}}$  exhibits a power-law distance dependence whose strength depends on the dielectric properties of the interacting colloidal particles and intervening medium. For spherical particles of equal size,  $V_{\text{vdW}}$  is given by the Hamaker expression:

$$V_{\text{vdW}} = -\frac{A}{6} \left( \frac{2}{s^2 - 4} + \frac{2}{s^2} + \ln \frac{s^2 - 4}{s^2} \right) \quad (2)$$

where  $s$  is

$$s = \frac{2a + h}{a} \quad (3)$$

and where  $h$  is the minimum separation between the particle surfaces,  $a$  the particle radius, and  $A$  the Hamaker constant.<sup>15,56</sup> Various methods of calculating  $A$  are described in a companion review by French<sup>57</sup> as well as in Refs. 58–60. Experimentally determined values for several important ceramic materials interacting under vacuum and across water are provided in Table I.<sup>59–61</sup> To account for retardation effects, use of a distance-dependent Hamaker function ( $A(h)$ ) is advised when interactions of interest exceed  $\sim 5$  nm.<sup>62,63</sup>

Long-range, attractive vdW forces between particles must be mitigated during colloidal processing to achieve the desired degree of suspension stability. One approach is to render this force negligible by suspending particles in an index-matched solvent. This has been demonstrated previously for silica and polymer-based lattices, which exhibit hard-sphere behavior in an appropriate nonaqueous solvent (refer to Fig. 2).<sup>64–66</sup> However, this approach is of limited practical importance because of the high index of refraction of most ceramic powders. One must therefore rely on some type of interparticle repulsion, such as electrostatic, steric, or depletion forces, to overcome the vdW attraction, as illustrated in Fig. 3.

## (2) Electrostatic Forces

The stability of aqueous colloidal systems can be controlled by generating like-charges of sufficient magnitude on the surfaces of suspended ceramic particles. The resulting repulsive  $V_{\text{elect}}$  exhibits an exponential distance dependence whose strength depends on the surface potential induced on the interacting colloidal particles and

the dielectric properties of the intervening medium. Exact analytical expressions for the electrostatic potential energy cannot be given; therefore, analytical approximations or numerical solutions are used. For spherical particles of equal size that approach one another under conditions of constant potential,  $V_{\text{elect}}$  is given by

$$V_{\text{elect}} = 2\pi\epsilon_r\epsilon_0a\Psi_0^2 \ln[1 + \exp(-\kappa h)] \quad (4)$$

provided  $\kappa a$  is sufficiently large ( $>10$ ). In contrast, when the double layer around each particle is extensive ( $\kappa a < 5$ ),  $V_{\text{elect}}$  is given by

$$V_{\text{elect}} = 2\pi\epsilon_r\epsilon_0a\Psi_0^2 \exp(-\kappa h) \quad (5)$$

where  $\epsilon_r$  is the dielectric constant of the solvent,  $\epsilon_0$  the permittivity of vacuum,  $\Psi_0$  the surface potential, and  $1/\kappa$  the Debye–Hückel screening length.  $\kappa$  is given by

$$\kappa = \left( \frac{F^2 \sum N_i z_i^2}{\epsilon_r \epsilon_0 k T} \right)^{1/2} \quad (6)$$

where  $N_i$  and  $z_i$  are the number density and valence of the counterions of type  $i$ , and  $F$  the Faraday constant.<sup>56</sup>  $\Psi_0$  results from the dissociation of amphoteric hydroxyl groups present on oxide surfaces and depends on pH and indifferent electrolyte concentration. It can be estimated from the zeta potential ( $\zeta$ ), which measures the electrostatic potential at, or very near to, the beginning of the diffuse double layer.

As predicted by DLVO theory, dispersions can be rendered unstable by either increasing ionic strength or adjusting pH toward the isoelectric point (IEP) (refer to Table II). For example, Lange and co-workers<sup>44,67</sup> produced weakly attractive, aqueous alumina suspensions at pH conditions below the IEP point and found that the yield strength increased with increased electrolyte concentration. These attractive networks were much weaker than those produced by flocculating the system at its IEP (pH  $\sim 8.5$ ). Because of the weak attraction between particles, such slurries could be consolidated under modest applied pressures to densities approaching those attainable in dispersed systems.<sup>67</sup> In contrast, Gauckler and co-workers<sup>46,47</sup> utilized enzymatic reactions to shift pH toward the IEP of the colloidal system of interest, thereby inducing coagulation, as shown in Fig. 4 (refer to Section V).

For multicomponent ceramic systems, it may be desirable to work in a pH range where opposite charges are induced on different colloidal phases. This approach, termed heteroflocculation, prevents unwanted phase segregation from occurring during processing. Lange *et al.*<sup>1</sup> demonstrated this effect in aqueous alumina–zirconia suspensions. When processed in a pH range below the respective IEPs of both phases (e.g., pH 2.5), the dispersed system underwent a dramatic phase segregation during centrifugal consolidation. However, at an intermediate pH ( $\sim 7$ ) between their respective IEPs, aggregation led to an intimate mixture of these phases that was not disrupted during consolidation.

Electrostatically stabilized suspensions are kinetically stable systems, where the rate of doublet formation is controlled by the stability ratio,  $W$ :

$$W = \frac{k_0}{k} \quad (7)$$

$$= \exp\left(\frac{V_{\text{max}}/k_b T}{2\kappa a}\right) \quad (8)$$

where  $V_{\text{max}}$  is the maximum repulsive barrier height,  $k_0$  the rate constant for fast irreversible flocculation ( $k_0 = 4k_b T/3\eta_0$ ), and  $k$  the rate constant of flocculation for the system of interest. The stability ratio exhibits an exponential dependence on  $V_{\text{max}}$  and a linear dependence on the normalized electrostatic double-layer thickness  $(\kappa a)^{-1}$ , as shown in Eq. (8). For an aqueous suspension containing 60 vol% solids (500 nm in diameter), a characteristic

**Table I. Nonretarded Hamaker Constants for Ceramic Materials Interacting under Vacuum and across Water at 298 K<sup>†</sup>**

Material	Crystal structure	Hamaker constant ( $\times 10^{-20}$ J)	
		Under vacuum	Across water
$\alpha$ -Al <sub>2</sub> O <sub>3</sub>	Hexagonal	15.2	3.67
BaTiO <sub>3</sub> <sup>‡</sup>	Tetragonal	18	8
BeO <sup>‡</sup>	Hexagonal	14.5	3.35
CaCO <sub>3</sub> <sup>‡</sup>	Trigonal	10.1	1.44
CdS	Hexagonal	11.4	3.4
MgAl <sub>2</sub> O <sub>4</sub>	Cubic	12.6	2.44
MgO	Cubic	12.1	2.21
Mica	Monoclinic	9.86	1.34
6H-SiC	Hexagonal	24.8	10.9
$\beta$ -SiC	Cubic	24.6	10.7
$\beta$ -Si <sub>3</sub> N <sub>4</sub>	Hexagonal	18.0	5.47
Si <sub>3</sub> N <sub>4</sub>	Amorphous	16.7	4.85
SiO <sub>2</sub> (quartz)	Trigonal	8.86	1.02
SiO <sub>2</sub>	Amorphous	6.5	0.46
SrTiO <sub>3</sub>	Cubic	14.8	4.77
TiO <sub>2</sub> <sup>‡</sup>	Tetragonal	15.3	5.35
Y <sub>2</sub> O <sub>3</sub>	Hexagonal	13.3	3.03
ZnO	Hexagonal	9.21	1.89
ZnS	Cubic	15.2	4.8
ZnS	Hexagonal	17.2	5.74
3Y-ZrO <sub>2</sub>	Tetragonal	20.3	7.23

<sup>†</sup>Reference 61. <sup>‡</sup>Average.

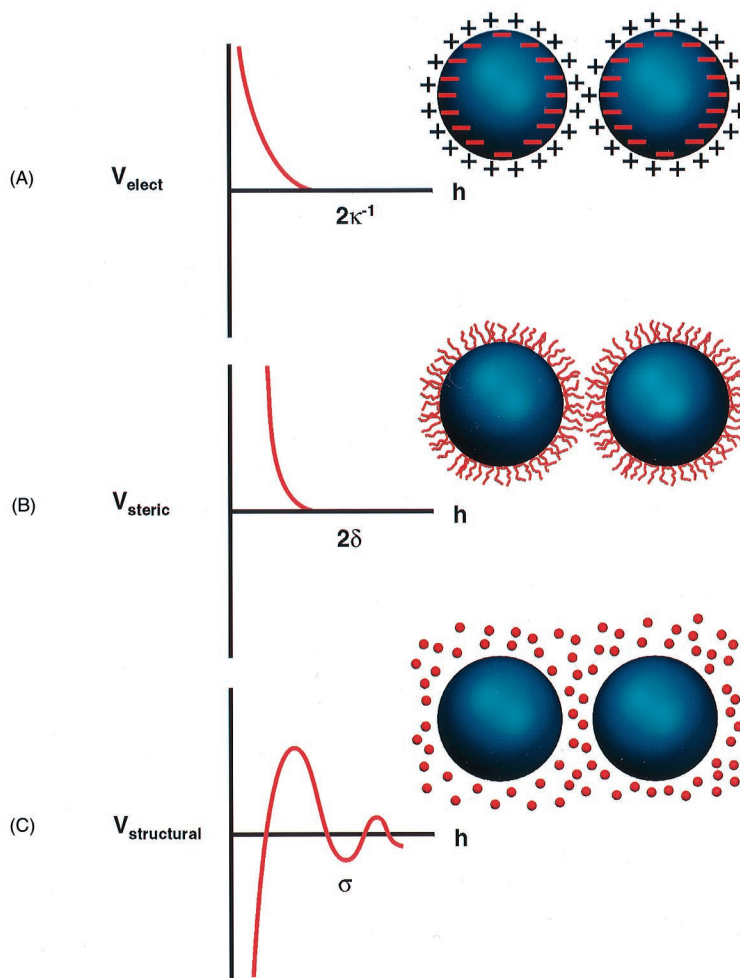


**Fig. 3.** Schematic illustration of the interaction potential energy and relevant length scales for (A) electrostatic, (B) steric, and (C) structural contributions, where  $\kappa^{-1}$  is the effective double-layer thickness,  $\delta$  the adlayer thickness, and  $a$  the characteristic size of species resulting in ordering within the interparticle gap. (For depletion forces,  $\sigma$  is approximately the depletant diameter, whereas, for solvation forces,  $\sigma$  is approximately the solvent diameter.)

**Table II. Isoelectric Points of Ceramic Materials<sup>†</sup>**

Material	IEP
$\alpha$ -Al <sub>2</sub> O <sub>3</sub>	8–9
3Al <sub>2</sub> O <sub>3</sub> ·2SiO <sub>2</sub>	6–8
BaTiO <sub>3</sub>	5–6
CeO <sub>2</sub>	6.7
Cr <sub>2</sub> O <sub>3</sub>	7
CuO	9.5
Fe <sub>3</sub> O <sub>4</sub>	6.5
La <sub>2</sub> O <sub>3</sub>	10.4
MgO	12.4
MnO <sub>2</sub>	4–4.5
NiO	10–11
SiO <sub>2</sub> (amorphous)	2–3
Si <sub>3</sub> N <sub>4</sub>	9
SnO <sub>2</sub>	7.3
TiO <sub>2</sub>	4–6
ZnO	9
ZrO <sub>2</sub>	4–6

<sup>†</sup>References 6 and 165.

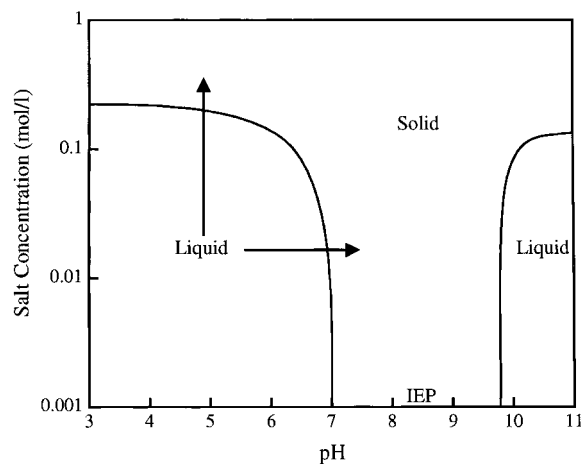


**Fig. 4.** Stability map of a concentrated aqueous alumina suspension as a function of varying pH and salt concentration. (Liquid  $\rightarrow$  solid transition can be promoted by either a shift in pH toward the IEP or an increase in ionic strength.) (Adopted from Refs. 46 and 47.)

aggregation time ( $t$ ) of  $\sim 0.02$  s is predicted for rapid flocculation, where  $t = 1/Nk_0$  and  $N$  the particle number density.<sup>68</sup> In the presence of a repulsive barrier, this characteristic time is extended considerably, as shown in Fig. 5. This analysis assumes a system in which only Brownian motion acts to bring particles together. During colloidal processing, external forces can “push” particles

over the repulsive barrier, further reducing suspension stability.<sup>2</sup> In practice, it may be difficult to effectively design stable suspensions based only on electrostatic stabilization. Particle solubility concerns may limit the working pH range, whereas an extended double-layer thickness may lead to unacceptable drying shrinkage.

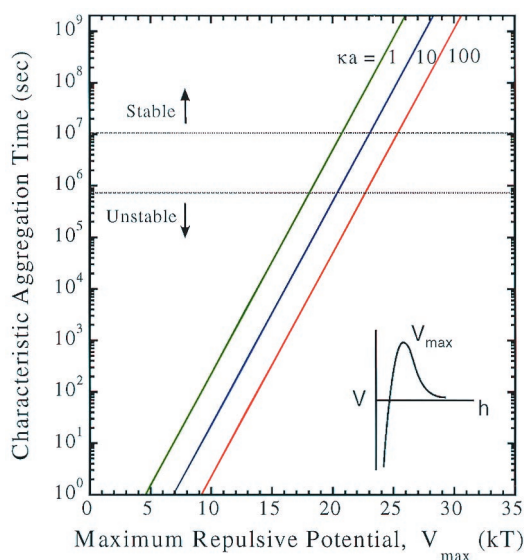


**Fig. 5.** Plot of characteristic aggregation time versus maximum repulsive potential for an aqueous ceramic suspension (60 vol% solids, 500 nm in diameter).

### (3) Steric Forces

Steric stabilization provides an alternate route of controlling colloidal stability that can be used in aqueous and nonaqueous systems. In this approach, adsorbed organic molecules (often polymeric in nature) are utilized to induce steric repulsion. To be effective, the adsorbed layers must be of sufficient thickness and density to overcome the vdW attraction between particles and to prevent bridging flocculation. Such species should be strongly anchored to avoid desorption during particle collisions. The conformation of adsorbed layers can vary dramatically, depending on solvent quality, molecular architecture, number of anchoring groups, active surface site density, and colloid and organic concentrations in solution.<sup>68</sup> As an example, schematic illustrations of such layers adsorbed on ideal ceramic surfaces are shown in Fig. 6 for varying molecular architectures, including homopolymers, diblock copolymers, comblike copolymers, and functionalized short-chain dispersants.

Steric interactions occur when particles approach one another at a separation distance less than twice the adlayer thickness ( $\delta$ ).

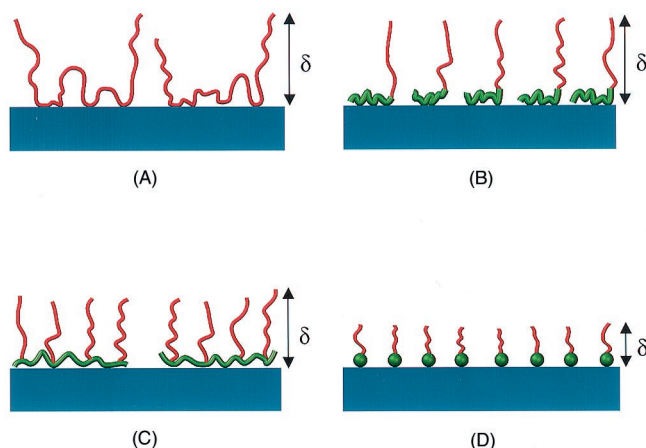


**Fig. 6.** Schematic illustrations of adlayer conformation on an ideal ceramic surface as a function of varying molecular architecture: (A) homopolymer, consisting of tails, loops, and train configuration; (B) diblock copolymer, consisting of short anchor block and extended chain block; (C) comblike copolymer, consisting of extended segments attached to anchored backbone; and (D) functional, short-chain dispersant, consisting of anchoring head group and extended tail.

Their close approach can be divided into two domains:<sup>1</sup> the interpenetrational domain ( $\delta < h < 2\delta$ )<sup>2</sup> and the interpenetrational-plus-compressional domain ( $h < \delta$ ).<sup>68</sup> When modeling homopolymer adsorption, a pseudohomopolymer model<sup>69</sup> is used to describe the mixing interactions that occur in the region,  $\delta < h < 2\delta$ , while the uniform segment model describes the mixing and elastic interactions that occur at smaller separations,  $h < \delta$ . The pseudohomopolymer model accounts for chain conformations other than tails (i.e., trains and loops) that are expected for such species. In the domain  $\delta < h < 2\delta$ ,  $V_{steric}$  is given by

$$V_{steric, mix} = \frac{32\pi a k_b T \bar{\phi}_2^a (0.5 - \chi)}{5v_1 \delta^4} \left( \delta - \frac{h}{2} \right)^6 \quad (9)$$

where  $\bar{\phi}_2^a$  is the average volume fraction of segments in the adsorbed layer measured as 0.37,  $\chi$  (the Flory–Huggins parameter) a measure of solvent quality,  $v_1$  the molar volume of solvent, and  $h$  the interparticle separation. At smaller interparticle separations (i.e.,  $h < \delta$ ), the polymer segment density is assumed to be uniform, and elastic contributions dominate the interaction potential energy. In this domain,  $V_{steric}$  is given by the sum of the mixing ( $V_{steric, mix}$ ) and elastic ( $V_{steric, el}$ ) terms:

$$V_{steric, mix} = \frac{4\pi a \delta^2 k_b T \bar{\phi}_2^a (0.5 - \chi)}{v_1} \left( \frac{h}{2\delta} - \frac{1}{4} - \ln \frac{h}{\delta} \right) \quad (10)$$

$$V_{steric, el} = \frac{2\pi a k_b T \delta^2 \rho_2 \bar{\phi}_2^a}{M_2^a} \left\{ \frac{h}{\delta} \ln \left[ \frac{h}{\delta} \left( \frac{3 - h/\delta}{2} \right)^2 \right] - 6 \ln \left( \frac{3 - h/\delta}{2} \right) + 3 \left( 1 - \frac{h}{\delta} \right) \right\}$$

where  $\rho_2$  is the density and  $M_2^a$  the molecular weight of the adsorbed species. Other adlayer configurations (e.g., block copolymers) are better modeled using alternate expressions provided in Ref. 69. As predicted, such dispersions can be rendered unstable when solvent conditions become poor (i.e.,  $\chi > 0.5$ ). Francis and co-workers<sup>70</sup> produced asymmetric ceramic–polymer membranes with controlled pore structures via coacervation by immersing samples in a poor solvent. Alternately, Bergström and Sjöström<sup>71</sup> induced reversible flocculation in nonaqueous ceramic suspensions by changing temperature, which also decreased solvency.

### (4) Electrosteric Forces

Polyelectrolyte species are widely used additives that can impart electrostatic and steric stabilization to a given colloidal dispersion.<sup>72</sup> Such systems are often referred to as electrosterically stabilized. Polyelectrolytes contain at least one type of ionizable group (e.g., carboxylic or sulfonic acid groups), with molecular architectures that range from homopolymers, such as poly(acrylic acid), to block copolymers with one or more ionizable segments. Polyelectrolyte adsorption is strongly influenced by the chemical and physical properties of the solid surfaces and solvent medium.<sup>73</sup> For example, adsorption is strongly favored when polyelectrolyte species and the colloid surfaces of interest carry opposite charges.<sup>74</sup> At small adsorbed amounts, such species can promote flocculation either via surface charge neutralization or bridging mechanisms. At higher adsorbed amounts, particle stability increases because of long-range repulsive forces resulting from electrosteric interactions.<sup>75</sup> For a given system, the adsorption behavior and conformation of polyelectrolyte species can be modulated by tailoring solvent conditions (e.g., pH and ionic strength). For anionic polyelectrolytes, the degree of ionization ( $\alpha$ ) increases with increasing pH.<sup>73,74,76</sup> Such species adopt a compact coil configuration in solution at low pH ( $\alpha \rightarrow 0$ ) and adsorb in a dense layer of large mass ( $\Gamma_{ads}$ ) and low adlayer thickness ( $\delta$ ), as shown in Fig. 7. In contrast, when fully ionized ( $\alpha \rightarrow 1$ ), anionic polyelectrolytes adopt an open coil configuration in solution because of intersegment repulsion. These highly charged species would adsorb in an open layer of low  $\Gamma_{ads}$  and high  $\delta$ , also shown in Fig. 7.<sup>73,76–78</sup> At

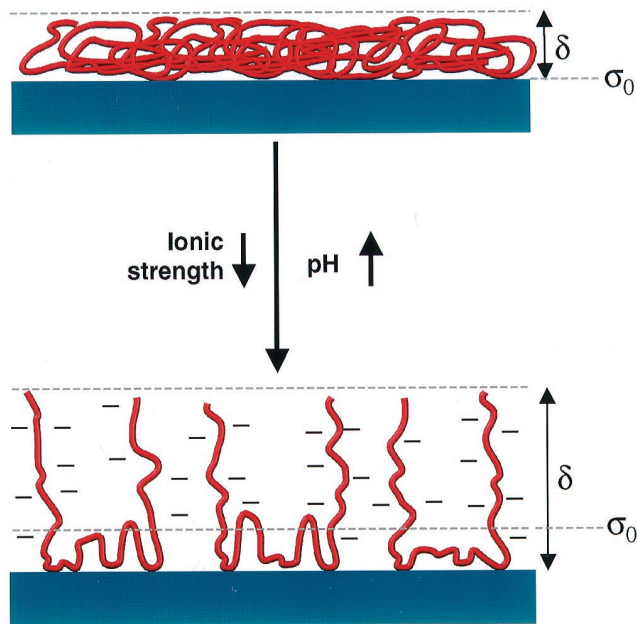


**Fig. 7.** Schematic illustration of adsorbed anionic polyelectrolyte species on an ideal ceramic surface as a function of pH and ionic strength ( $\delta$  is the adlayer thickness and  $\sigma_0$  the plane of charge).

high ionic strength, however, screening effects can mitigate intersegment repulsion altering adlayer structure.<sup>74,75</sup>

To accurately model colloidal interactions in the presence of polyelectrolyte species, assignments of the vdW plane, the plane of charge ( $\sigma_0$ ), and the steric interaction length ( $\delta$ ) are of critical importance (refer to Fig. 7). Theoretical treatments of such interactions have varied significantly from assuming that double layer, vdW, and steric forces all originate at the polyelectrolyte–solution interface<sup>79</sup> to assuming that double layer and vdW forces originate at the solid–polyelectrolyte interface and steric forces originate at the polyelectrolyte–solution interface.<sup>80</sup> Recently, Biggs and Healy<sup>73</sup> directly measured such interactions between zirconia surfaces with adsorbed poly(acrylic acid) (MW  $\approx$  2000 g/mol) using atomic force microscopy (AFM). At low pH ( $\alpha \rightarrow 0$ ), they observed that the steric interaction length and calculated plane of charge (estimated from the normalized force versus separation distance curves) were coincident and occurred  $\sim 1$  nm away from the bare particle surfaces. As pH increased, they observed a dramatic increase in the steric interaction length, with almost a 10-fold increase ( $\delta \approx 10$  nm) at pH 9. Simultaneously, they found a more modest shift for the calculated plane of charge away from the particle surface, which doubled to  $\sim 2$  nm under the same pH conditions. As their results illustrate, the plane of charge is often located at some intermediate distance between the solid–polyelectrolyte and polyelectrolyte–solution interfaces. One would expect this location to depend strongly on the polyelectrolyte architecture and solution properties of a given system.

### (5) Depletion Forces

Depletion forces occur between large colloidal particles suspended in a solution of nonadsorbing, smaller species (e.g., polymers, polyelectrolytes, or fine colloidal particles). Such species, known as depletants, may promote flocculation or stabilization of primary colloidal particles. Depletion denotes the existence of a negative depletant concentration gradient near primary particle surfaces. The concentration of rigid depletant species decreases at bare particle surfaces and increases to its bulk solution value at some distance away from these surfaces. This distance, known as the depletion layer thickness, is of the order of the depletant diameter ( $2a_{\text{dep}}$ ). Recent theoretical<sup>81,82</sup> and experimental<sup>83</sup> evidence has revealed that the depletion force has the same origin and form as structural (solvation) forces.<sup>84–86</sup> Despite their low

concentration in solution relative to solvent species, depletant effects on suspension stability can be quite dramatic.<sup>63</sup> This results because of the characteristic length scale of such interactions, which can be several nanometers or greater, depending on the effective depletant diameter (refer to Table III). For uncharged depletant species,  $V_{\text{dep}}$  is given by<sup>82</sup>

$$V_{\text{dep}}(\lambda) = 0 \quad \text{for } h > 2a_{\text{dep}}$$

$$V_{\text{dep}}(\lambda) = \frac{a\phi_{\text{dep}}^2 kT}{10a_{\text{dep}}} (12 - 45\lambda + 60\lambda^2 - 30\lambda^3 + 3\lambda^5) \quad \text{for } 4a_{\text{dep}} > h \geq 2a_{\text{dep}}$$

$$V_{\text{dep}}(\lambda) = -\frac{3a\phi_{\text{dep}} kT}{2a_{\text{dep}}} + \frac{a\phi_{\text{dep}}^2 kT}{10a_{\text{dep}}} (12 - 45\lambda - 60\lambda^2) \quad \text{for } h < 2a_{\text{dep}} \quad (11)$$

where  $\phi_{\text{dep}}$  is the depletant volume fraction in solution and  $\lambda = (h - 2a_{\text{dep}})/2a_{\text{dep}}$ . This expression accounts for second-order concentration effects and assumes that the depletant species can be modeled as rigid, uniform spheres. Interactions resulting from the presence of charged depletant species (e.g., nonadsorbed polyelectrolytes or fine colloidal particles) would be better modeled by the equations provided in Ref. 81.

Otherwise stable dispersions are known to undergo transitions from stable  $\rightarrow$  depletion flocculation  $\rightarrow$  depletion restabilization with increasing depletant volume fraction.<sup>69,87,88</sup> Destabilization occurs when such species are excluded from the interparticle gap, resulting in an osmotic pressure difference that promotes flocculation.<sup>19,20</sup> Ogden and Lewis<sup>63</sup> recently conducted the first systematic study of depletant effects on the stability of weakly flocculated, concentrated colloidal suspensions. Their observations have shown that the stability of such systems *only improves* with increasing depletant additions. Such observations were attributed to the presence of a repulsive barrier (estimated to be of the order of  $kT$  or greater), occurring before the exclusion of depletant species from the gap region (refer to Fig. 3(C)). Clearly, the net impact of depletion forces depends strongly on the initial system stability in the absence of such species.

## VI. Suspension Rheology

The rheological behavior of colloidal dispersions is among their most important properties.<sup>89</sup> Rheological measurements monitor changes in flow behavior in response to an applied stress (or strain). Suspension, structure, and, hence, stability can be inferred from the observed behavior. The critical parameters of interest include the apparent viscosity ( $\eta$ ), the yield stress under shear ( $\tau_y$ ) and compression ( $P_y$ ), and the viscoelastic properties (i.e., the loss ( $G''$ ) and elastic ( $G'$ ) moduli) of the system. Such parameters must be tailored for the specific forming method used during ceramics processing (refer to Section V). Most emerging forming routes require concentrated colloidal systems, with  $\phi$  approaching 0.6. Although this is readily achieved in model hard-sphere systems, ceramic suspensions often consist of irregularly shaped particles with adsorbed and/or nonadsorbed processing aids that serve to effectively decrease the solids loading.

**Table III.** Typical Dimensions of Nonadsorbed Polymer Species in Solution<sup>†</sup>

Molecular weight (g/mol)	Characteristic size (nm)
$10^3$	2
$10^4$	6
$10^5$	20
$10^6$	60

<sup>†</sup>Reference 68.

### (I) Types of Flow Behavior

(A) *Viscous Flow Behavior:* The apparent viscosity ( $\eta$ ) is related to the applied shear stress ( $\tau$ ) and shear rate ( $\dot{\gamma}$ ) by the following expression:

$$\tau = \eta \dot{\gamma} \quad (12)$$

Various types of flow behavior can be observed under steady shear depending on suspension composition and stability, as shown in Fig. 8. Newtonian behavior is the simplest flow response, where viscosity is independent of shear rate (see curve (a) in Fig. 8). Pseudoplastic or shear-thinning behavior occurs when the viscosity decreases with shear rate (see curve (b)). This response can be accompanied by a yield stress whose magnitude depends on the strength of the particle network (see curves (d) and (e)). If the flow curve is linear above  $\tau_y$ , the system is referred to as Bingham plastic (curve (d)). Finally, dilatant or shear-thickening behavior occurs when the viscosity increases with shear rate (see curve (c)). The rheological properties of concentrated colloidal suspensions are often time dependent. Thixotropic systems exhibit an apparent viscosity that decreases with time under shear, but recovers to its original viscosity when flow ceases. The opposite behavior is referred to as rheopexy.

(B) *Viscoelastic Behavior:* Concentrated colloidal suspensions commonly display viscoelastic behavior, which can be characterized by dynamic rheological measurements (or oscillatory techniques). During oscillation measurements, a frequency-dependent shear stress or strain is applied to a suspension, and the shear moduli are obtained. The complex shear modulus ( $G^*$ ) has a real and an imaginary component, as given by

$$G^* = G' + iG'' \quad (13)$$

where  $G' = G^* \cos \delta$ ,  $G'' = G^* \sin \delta$ , and  $\delta$  is the phase angle. When the applied strain and resulting stress are in phase ( $\delta = 0$ ), energy is completely stored; i.e., the suspension is purely elastic (solidlike). If the applied strain and resulting stress are fully out of phase ( $\delta \approx 90^\circ$ ), energy is completely dissipated; i.e., the suspension is purely viscous (liquidlike). In the intermediate range  $0^\circ < \delta < 90^\circ$ , the suspension exhibits a viscoelastic response.

Colloidal suspensions are usually characterized by oscillatory measurements in the linear viscoelastic regime (at small shear stresses or strains) to examine their behavior in the least perturbed state. The limit of the linear viscoelastic regime is defined as the shear stress (or strain) where the shear modulus deviates from its low shear plateau value. Structural information is obtained by conducting frequency ( $\omega$ ) sweeps at a given stress (or strain) in this regime, as shown in Fig. 9. A liquidlike response is observed when  $G'' > G'$  over the entire frequency spectrum;  $G'$  and  $G''$  vary as  $\omega^2$  and  $\omega$ , respectively, as  $\omega \rightarrow 0$ . A gellike response is observed when  $G'$  and  $G''$  vary as  $\omega^j$ , where  $j = 0.3-0.7$ , depending on the system. Finally, a solidlike response is observed when  $G' > G''$  over the entire frequency spectrum, where  $G'$  is independent of frequency as  $\omega \rightarrow 0$ .<sup>90</sup>

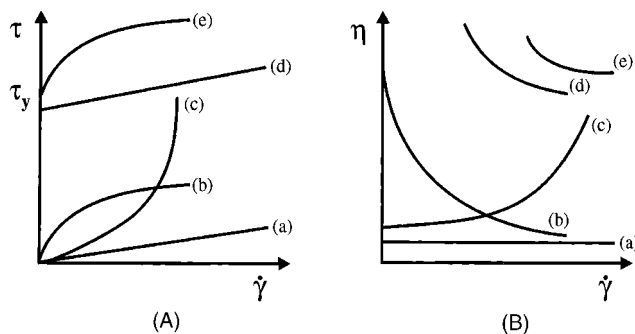


**Fig. 8.** Types of rheological behavior exhibited by colloidal dispersions: (a) Newtonian flow; (b) shear thinning; (c) shear thickening; (d) Bingham plastic; and (e) pseudoplastic with a yield stress.

(C) *Compressive Flow Behavior:* Compressive rheology, pioneered by Buscall,<sup>91</sup> allows one to determine the osmotic pressure ( $\Pi(\phi)$ ) for dispersed systems and compressive yield stress ( $P_y(\phi)$ ) for flocculated systems that must be overcome to promote consolidation. Several techniques can be used to measure the compressive flow behavior of colloidal suspensions, including gravitational sedimentation,<sup>3,41</sup> pressure filtration,<sup>92</sup> osmotic consolidation,<sup>92</sup> and centrifugation.<sup>3,92-94</sup> In centrifugation, this property can be assessed by measurement of either sediment height at multiple spinning speeds, volume fraction profile during centrifugation by destructive sectioning, or  $\gamma$ -ray densitometry. A schematic illustration of the coordinate system for the centrifugation method is shown in Fig. 10. The stress acting on any position  $z$  in the network is given by<sup>91-93</sup>

$$P(z) = \int_z^{H_{eq}} \Delta \rho g(z) \Phi(z) dz \quad (14)$$

where  $g(z)$  is the acceleration,  $\Delta \rho$  the density difference between the particulate phase and the suspending medium, and  $\Phi(z)$  the local volume fraction of solids at height  $z$ . Equilibrium is attained when the suspension has consolidated to a given volume fraction such that the applied stress ( $P$ ) is balanced by the osmotic pressure or compressive yield stress of the system.

### (2) Effect of Interparticle Forces on Flow Behavior

(A) *Hard-Sphere Systems:* Hard-sphere colloidal suspensions do not experience interparticle interactions until the point of contact ( $h = 0$ ), when the interaction is infinitely repulsive (refer to Fig. 2). Such systems represent the simplest case, whose structure is dictated only by hydrodynamic (viscous) interactions and Brownian motion. Realistically, there are few truly hard-sphere suspensions. However, model systems, such as silica spheres stabilized by adsorbed stearyl alcohol layers in cyclohexane<sup>64,65</sup> and poly(methyl methacrylate) latices stabilized with poly(12-hydroxystearic acid) in a hydrocarbon mixture,<sup>66</sup> have been shown to approach this behavior. These model systems serve as a benchmark for assessing the more complicated behavior that occurs in the presence of interparticle forces. The relative viscosity ( $\eta_{rel} = \eta/\eta_0$ ) of hard-sphere systems has been shown to scale with the Peclet number (Pe) which is defined as

$$Pe = \frac{a^3 \eta_0 \dot{\gamma}}{k_b T} \quad (15)$$

where  $\eta_0$  is the solution viscosity. Pe characterizes the relative importance of viscous and Brownian contributions. Typically, viscous forces begin to dominate when Pe is approximately unity, which correlates with the onset of shear-thinning behavior.

Hard-sphere systems exhibit Newtonian flow at low solids loading ( $\phi < 0.3$ ). When  $\phi > 0.3$ , low- and high-shear Newtonian plateaus separated by a region of shear thinning are observed. Shear thinning occurs because of the hydrodynamic interactions of rotating doublets, which eventually break up, thereby reducing viscosity.<sup>95</sup> Shear thickening also has been observed in such systems at elevated volume fractions. This has been attributed to either an order-disorder structural transition<sup>38,96-98</sup> or cluster formation.<sup>39</sup> Finally, as  $\phi \rightarrow 0.6$ , a yield stress has been observed that results from the structural disruption accompanying particle movement in dense suspensions.

The effect of solids loading on the flow behavior of hard-sphere suspensions has been well studied. For dilute systems, the Einstein relationship describes the relative viscosity dependence on colloid volume fraction  $\phi$ :

$$\eta_{rel} = 1 + 2.5\phi \quad (16)$$

At higher concentrations ( $\phi > 0.05$ ), hydrodynamic and Brownian many-body interactions affect rheological behavior. In this regime, the Krieger-Dougherty model can be used to describe this dependence:<sup>95</sup>

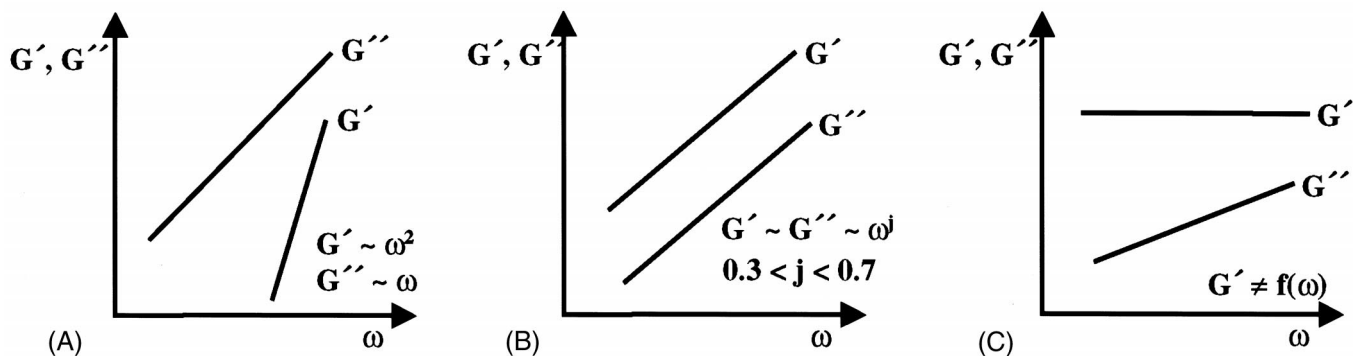


Fig. 9. Schematic representation of oscillatory behavior as a function of frequency for (A) liquid, (B) gel, and (C) solid response.

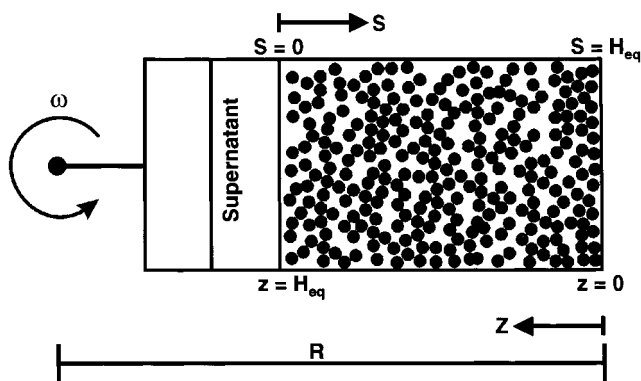


Fig. 10. Schematic illustration of the coordinate system used in the centrifugation technique for compressive rheology measurements.

$$\eta_{rel} = \left(1 - \frac{\phi}{\phi_{max}}\right)^{-K\phi_{max}} \quad (17)$$

where  $K = 2.5$  for monodisperse spheres and  $\phi_{max}$  is the maximum solids loading. As  $\phi \rightarrow \phi_{max}$ , the relative viscosity increases dramatically, as shown in Fig. 11. By tailoring particle-size distribution, one can achieve higher maximum solids loading than possible in monomodal systems, where  $\phi_{max} \approx 0.6-0.64$ .

The viscoelastic properties of hard-sphere systems exhibit the following scaling behavior:

$$G'_d = \frac{G' a^3}{k_b T}$$

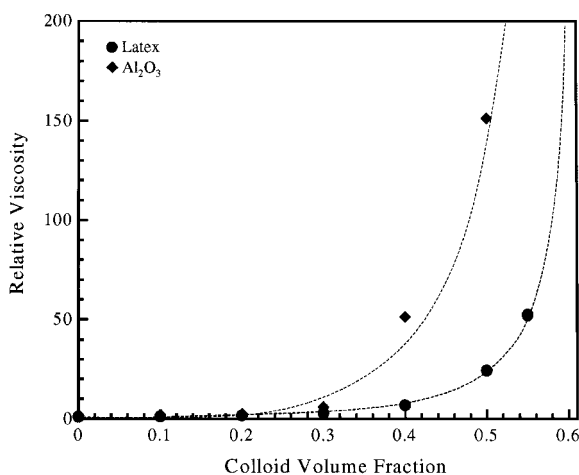


Fig. 11. Plot of relative viscosity as a function of colloids volume fraction in suspension.

$$G''_d = \frac{G'' a^3}{k_b T}$$

$$\omega_d = \frac{\eta_0 \omega a^3}{k_b T} \quad (18)$$

where  $G'_d$ ,  $G''_d$ , and  $\omega_d$  are the dimensionless dynamic storage modulus, loss modulus, and frequency, respectively.<sup>99</sup>

Molecular dynamic simulations of hard-sphere suspensions indicate that the osmotic pressure is negligible until the random close-packing limit is approached.<sup>100</sup> Guo and Lewis<sup>3</sup> found that the osmotic pressure ( $\Pi$ ) dependence on colloid volume fraction can be modeled using a modified Carnahan–Starling equation:

$$\Pi(\phi) = \frac{RT \phi (1 + \phi + \phi^2 - \phi^3)}{\bar{V} (\phi_{max} - \phi)^3} \quad (19)$$

where  $\bar{V}$  is the molar volume of the colloid phase. Using Eq. (19),  $\phi_{max} = 0.639$  was predicted for dispersed silica suspension behavior shown in Fig. 12.

(B) *Soft-Sphere Systems*: Most ceramic suspensions can be classified as soft-sphere systems; i.e., repulsive interactions occur some characteristic distance away from the particle surface (refer to Fig. 2). For electrostatically and sterically stabilized systems, this distance is given by the electric double-layer and adlayer thickness, respectively. Depending on the strength of these interactions relative to vdW forces, such systems may exhibit dispersed to weakly attractive behavior. Stable, soft-sphere systems have

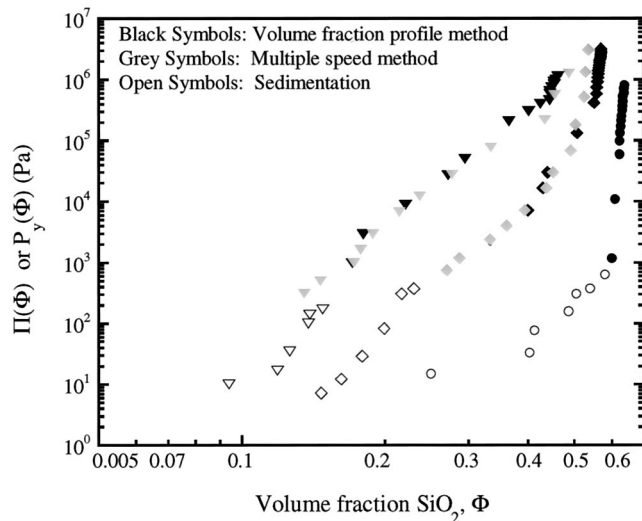


Fig. 12. log–log plot of osmotic pressure and compressive yield stress as a function of solids volume fraction for silica suspensions of varying stability: (A) dispersed; (B) weakly flocculated; and (C) strongly flocculated. (As these data illustrate, there is little variation between the various compressive rheology methods.) (Adopted from Ref. 3.)

been shown to display flow behavior similar to that described above for hard-sphere systems. Hard-sphere scaling has been successfully applied in systems of particles with relatively thin layers (i.e., low  $\delta/a$  ratios), provided the adsorbed layer has been accounted for in an effective volume fraction ( $\phi_{\text{eff}}$ ).  $\phi_{\text{eff}}$  is enhanced by the volume occupied by the soft layer around each particle, according to<sup>89</sup>

$$\phi_{\text{eff}} = \phi \left( 1 + \frac{\delta}{a} \right)^3 \quad (20)$$

Equation (20), valid for spherical colloids, can be modified to account for irregularly shaped particles, as follows:

$$\phi_{\text{eff}} = \phi \left( 1 + \frac{\rho_s \delta A_s}{a} \right)^3 \quad (21)$$

where  $\rho_s$  is the powder density ( $\text{g/m}^3$ ) and  $A_s$  the specific surface area of the ceramic powder ( $\text{m}^2/\text{g}$ ).<sup>63</sup> As shown in Fig. 13, the presence of adsorbed processing aids can dramatically reduce the actual solids loading in suspension.

(C) *Flocculated Systems:* Flocculated suspensions are dominated by attractive interparticle forces and tend to form disordered, metastable structures with varying relaxation times. Weakly attractive interactions occur in systems with a shallow secondary minimum ( $1 < -V_{\text{min}}/k_b T < 20$ ). This behavior can be induced by adding nonadsorbed polymer to an otherwise stable suspension,<sup>87,88</sup> or by flocculation into a secondary minimum in the DLVO potential,<sup>40,44</sup> or combined vdW and steric potentials.<sup>63</sup> An aggregated-particle network forms in suspension at volume fractions  $\geq \phi_{\text{gel}}$ , where  $\phi_{\text{gel}}$  depends on the relative strength of the interparticle attraction. Such systems exhibit reversible flocculation, which facilitates structural deformation during flow and reformation on the cessation of flow. With increasing shear stress (or strain), the “links” between particle clusters or individual particles are disrupted. As a result, substantial shear-thinning behavior is observed at low stresses and solids loadings ( $\phi \ll 0.6$ ). In contrast, strongly attractive interactions occur in systems that flocculate into a deep minimum ( $-V_{\text{min}}/k_b T > 20$ ). In this case, flocculation is irreversible. These systems exhibit strong shear-thinning behavior as well as a substantial yield stress and shear modulus when  $\phi = \phi_{\text{gel}} \approx 0.05$ .

Above the gel point ( $\phi > \phi_{\text{gel}}$ ), strongly flocculated suspensions display a yield stress ( $\tau_y$ ) that exhibits a power-law dependence on solids loading:<sup>101</sup>

$$\tau_y \approx \phi^n \quad (22)$$

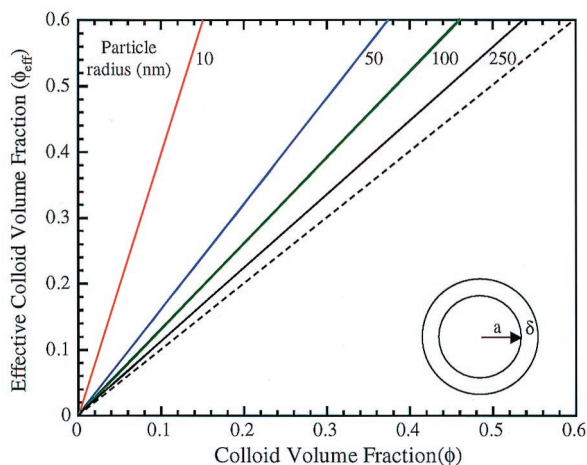


**Fig. 13.** Effective colloid volume fraction as a function of actual colloid volume in solution for soft-sphere colloids of varying radii and constant adlayer thickness ( $\delta = 10$  nm and (---) behavior of hard-sphere systems, where  $\delta = 0$ ).

where  $n = 2.5$ – $3$ . Similarly, the shear moduli also exhibit a power-law dependence:

$$G' \approx \phi^m \quad (23)$$

where  $m \approx 4$ . This value is consistent with the exponent obtained in simulations of viscoelastic behavior in systems displaying diffusion-limited aggregation, where  $m \approx 3.5$ .<sup>101</sup>

In flocculated systems, stress is transmitted through a space-filling, aggregated particle network formed when the colloid volume fraction exceeds the gel point ( $\phi_{\text{gel}}$ ).<sup>41</sup> This stress, defined as the compressive yield stress ( $P_y(\phi)$ ), increases rapidly with  $\phi$ .<sup>36</sup> Previous studies have shown that  $P_y(\phi)$  is well described by a power-law function, when  $\phi > \phi_{\text{gel}}$ . Because the mechanical properties of the systems were similar at  $\phi_{\text{gel}}$ , Landman and White<sup>102</sup> suggested that the compressive yield stress of flocculated systems of varying network strength should exhibit universal behavior when normalized by their respective  $\phi_{\text{gel}}$ , as follows:

$$P_y(\phi) = b \left( \frac{\phi}{\phi_{\text{gel}}} - 1 \right)^n \quad (24)$$

where the gel point varies inversely with the strength of the interparticle attractions.<sup>36,41</sup> This has been confirmed by Zukoski and co-workers<sup>92,103</sup> for flocculated ceramic suspensions. Alternatively, Buscall *et al.*<sup>36</sup> have shown that flocculated systems of submicrometer spheres displayed a  $P_y(\phi)$  that exhibits the following power-law dependence:

$$P_y(\phi) = b\phi^n \quad (25)$$

where  $n = 4 \pm 0.5$ . Because the particle network strengthens dramatically with increased volume fraction and degree of interparticle attraction, it is difficult to completely consolidate flocculated systems under modest applied loads ( $\leq 1$  MPa), as shown in Fig. 12.

## V. Colloidal Consolidation Techniques

Consolidation of colloidal suspensions into dense, homogeneous green bodies is a central feature of colloidal processing. To exploit the advantages of this approach, it is desirable to form bodies directly from the slurry state.<sup>1</sup> Once shaped, the rheological properties of the as-formed body must be altered dramatically to permit demolding (when necessary) and subsequent handling without shape deformation. Solidification can be induced via fluid removal, particle flow (or compaction), or gelation. Several colloidal routes have been developed to produce ceramic components of varying geometric shape, complexity, and microstructural control, as shown in Table IV. Their salient features are outlined below.

### (1) Consolidation via Fluid Removal

Particle consolidation into a dense layer or body accompanies fluid removal in several forming routes, including pressure filtration,<sup>104–106</sup> slip casting,<sup>106–108</sup> osmotic consolidation,<sup>92,109</sup> tape casting,<sup>110–112</sup> and robocasting.<sup>52</sup> During pressure filtration, slip casting, and osmotic consolidation, a portion of the liquid vehicle is removed to yield a saturated ceramic body that must undergo subsequent drying. During tape casting and robocasting, shaping and drying processes occur simultaneously. During pressure filtration, a dense particulate layer is formed at the suspension–filter interface, as fluid flows through the filter in response to an applied pressure. In contrast, the other forming routes rely on a chemical potential gradient applied to the liquid phase to induce fluid removal. In slip casting, for example, fluid flows into a porous gypsum mold via capillary-driven transport. In osmotic consolidation, developed by Zukoski and co-workers,<sup>92,109</sup> a suspension is immersed in a polymer solution separated by a semipermeable membrane, through which fluid flows in response to an osmotic

**Table IV. Representative Colloidal-Forming Routes Classified by Consolidation Mechanism**

Forming method	Consolidation mechanism	Component shape
	A. Fluid removal	
Slip casting	Fluid flow into porous mold driven by capillary forces	Complex, 3D, thin walled
Pressure filtration	Fluid flow through porous filter driven by an applied pressure	Simple, 3D
Osmotic consolidation	Fluid flow through a semipermeable membrane driven by osmotic pressure difference	Simple, 3D
Tape casting	Fluid removal due to evaporation	Simple, 2D, thin layers
Robocasting <sup>†</sup>	Fluid removal due to evaporation	Complex, 3D
	B. Particle flow	
Centrifugal consolidation	Particle flow due to applied gravitational force	Complex, 3D
Electrophoretic deposition	Particle flow due to applied electric field	Simple, 2D or 3D
	C. Gelation	
Aqueous injection molding (AIM)	Physical organic gel forms in response to a temperature change	Complex, 3D
Gelcasting	Cross-linked organic network forms because of chemical reaction	Complex, 3D
Direct coagulation casting (DCC)	Colloidal gel forms because of flocculation	Complex, 3D
Robocasting <sup>†</sup>	Colloidal gel forms because of flocculation	Complex, 3D

<sup>†</sup>Solid freeform fabrication technique (consolidation can be induced via mechanism A or C).

pressure:

$$\Pi_{\text{poly}} = \frac{\mu_0 - \mu_{\text{poly}}}{V_m} \quad (26)$$

where  $\Pi_{\text{poly}}$  is osmotic pressure of the polymer solution,  $\mu_0$  the chemical potential of the solvent without added polymer,  $\mu_{\text{poly}}$  the chemical potential of the solvent with added polymer, and  $V_m$  the solvent molar volume. During drying, fluid is removed via evaporative processes (refer to Section VI). Experimental work by the groups of Zukoski<sup>92</sup> and Lewis<sup>3</sup> demonstrated that particle-packing densities rivaling those achieved under applied mechanical loads, e.g., pressure filtration,<sup>67,113</sup> are possible via chemically driven consolidation.

Tape casting produces a thin layer of composite material by coating a carrier surface with a ceramic suspension using the doctor-blade technique.<sup>110–112,114,115</sup> The applied coating dries to form a flexible film that consists of a particle-filled, polymer matrix. This technique yields flat, thin ceramic sheets with thicknesses between 10 and 1000  $\mu\text{m}$ . Such layers serve as the basic building blocks of multilayer ceramic packages (MLCs) and capacitors (MCCs).<sup>116,117</sup> Tape-cast layers also serve as feedstock for laminated-based solid freeform fabrication techniques, such as CAM-LEM.<sup>54</sup>

Robocasting<sup>52</sup> produces three-dimensional components in a layer-by-layer build sequence that involves computer-controlled deposition of a concentrated colloidal suspension ( $\phi > 0.5$ ). After minimal drying, the deposited suspension undergoes a liquid to solid transition that “freezes” in the as-patterned structure. Robocasting is the only SFF technique developed to date that utilizes colloidal systems of low organic content to directly write three-dimensional bodies. Current challenges to this approach involve controlling macroscopic shape evolution during deposition to avoid unwanted deformation. In a collaborative effort between the Cesarano and Lewis research groups, colloidal gels and colloid-filled hydrogels<sup>50,118</sup> have been developed with controlled rheological properties. Such colloid-based feedstocks yield deposited layers with optimized flow behavior (e.g.,  $\eta$  and  $\tau_y$ ) that allow complex architectures to be fabricated (see Panel A).

## (2) Consolidation via Particle Flow

Particle consolidation into a dense layer or body occurs via particle flow in response to an applied force in several forming routes, including sedimentation,<sup>34,41,42,119–121</sup> centrifugation,<sup>122–124</sup> and electrophoretic deposition.<sup>125–127</sup> Particles flow in response to gravitational forces during sedimentation and centrifugation. Sedimentation of suspended particles has been studied extensively because of its importance in many industrial processes. A spherical particle of density  $\rho_s$  and radius  $a$  released into a viscous fluid of viscosity  $\eta_0$  and density  $\rho$  momentarily accelerates and then decreases at a constant terminal velocity  $U_0$ . Laminar flow occurs

when the Reynolds number ( $\text{Re}$ ) is  $< 0.2$ , where  $\text{Re} = U_{0ap}/\eta_0$ . For ceramic particles, the upper size limit is  $\sim 50 \mu\text{m}$ . In the dilute limit ( $\phi > 0$ ), the settling (or terminal) velocity is determined by balancing opposing viscous and gravitational forces:

$$U_0 = \frac{2}{9} \frac{(\rho_s - \rho)}{\eta_0} a^2 g \quad (27)$$

which yields the well-known Stokes law. For concentrated suspensions, the settling velocity  $U$  is affected by hydrodynamic interactions with neighboring particles, which is significant if their separation distance is of the order of the particle size or less. In this case,  $U$  exhibits a Richardson–Zaki form:<sup>121</sup>

$$\frac{U}{U_0} = (1 - \phi)^n \quad (28)$$

where  $n = 6.55$ . Guo and Lewis<sup>40</sup> demonstrated that the sedimentation behavior of concentrated, monodisperse colloidal silica dispersions could be well described by Eq. (28). For stable suspensions, centrifugation simply enhances the rate of particle consolidation by increasing the applied gravitational force.

The behavior of flocculated suspensions is more complicated and not well described by hard-sphere constitutive responses.<sup>128</sup> For example, gravity-driven consolidation behavior of flocculated systems depends strongly on solids volume fraction  $\phi$ . In dilute suspensions, aggregation produces discrete clusters that settle more or less independently. Above some critical volume fraction, known as the gel point ( $\phi_{\text{gel}}$ ), the clusters become overcrowded, and an inhomogeneous space-filling network (or gel) forms, which may or may not consolidate, depending on its strength.<sup>41</sup> Recently, Allain *et al.*<sup>34</sup> studied simultaneous aggregation and sedimentation in colloidal suspensions and developed a model for relating the settling dynamics of gelled networks to their specific spatial structure. Their work is useful in understanding the various transitions from settling of isolated clusters at  $\phi < \phi_{\text{gel}}$ , to collective settling of a gel network at  $\phi \geq \phi_{\text{gel}}$ , to no settling when  $\phi$  approaches an upper critical limit (i.e., when the gel network formed can support itself). Zukoski and co-workers<sup>92,103</sup> studied centrifugal consolidation of aggregated ceramic suspensions to determine  $P_y(\phi)$  curves for gelled systems of varying composition, particle size, and attractive network strength. They showed that the applied loads needed to promote consolidation to a given  $\phi$  increase dramatically with decreasing particle size and/or increasing attractive network strength.

In electrophoretic deposition (EPD), particles flow in response to an applied direct-current (dc) electric field.<sup>127</sup> Under dc bias, charged colloidal particles move toward, and, ultimately deposit on, an oppositely charged electrode to produce a consolidated layer or body. The electrophoretic velocity ( $U_e$ ) is determined by

### Panel A. Robotically Controlled Deposition of Ceramics

Solid freeform (SFF) fabrication routes offer the ability to produce complex ceramic components that are not otherwise achievable by conventional forming methods. Here, we describe our recent collaborative efforts to design novel periodic structures for functional ceramics (e.g., 3–3 composites) via robotically controlled deposition<sup>52,162</sup> (see Fig. A–1). This example illustrates the important relations between colloidal stability, rheological behavior, and ceramics fabrication.

To produce spanning structures with excellent shape retention, one must use highly concentrated colloidal suspensions ( $\phi \rightarrow \phi_{\text{max}}$ ) with the appropriate flow properties. Important properties that must be tailored include suspension viscosity ( $\eta$ ) under the shear conditions experienced during deposition and yield stress ( $\tau_y$ ) of the as-deposited material. We have found that colloidal gels that can be made to flow under high shear but have a substantive yield stress (and, hence, infinite viscosity) under low shear conditions are most desirable.

Fluid-flow modeling conducted by Baer and co-workers<sup>118</sup> indicates that shear rates between 1 and 250  $\text{s}^{-1}$  are experienced during deposition from the nozzle tip (see Fig. A–2). By tailoring the relative strength of electrostatic interactions, Smay *et al.*<sup>163</sup> have developed aqueous suspensions of lead zirconate titanate with the range of  $\eta$  and  $\tau_y$  values depicted in Fig. A–3. The flow properties required to produce spanning structures are denoted by the upper region in Fig. A–3. Using these suspensions, we fabricated the representative, three-dimensional periodic structure shown in Fig. A–4. In this example, a highly concentrated lead zirconate titanate suspension (53 vol% solids) was deposited from a nozzle tip (diameter of  $\sim 800 \mu\text{m}$ ) to build a face-centered tetragonal lattice. Because of their high  $\tau_y$  values, the as-deposited beads maintained their cylindrical shape during deposition and drying. In addition to the highlighted work, this processing technology can be exploited to build a broad range of novel structures with controlled architecture and composition.

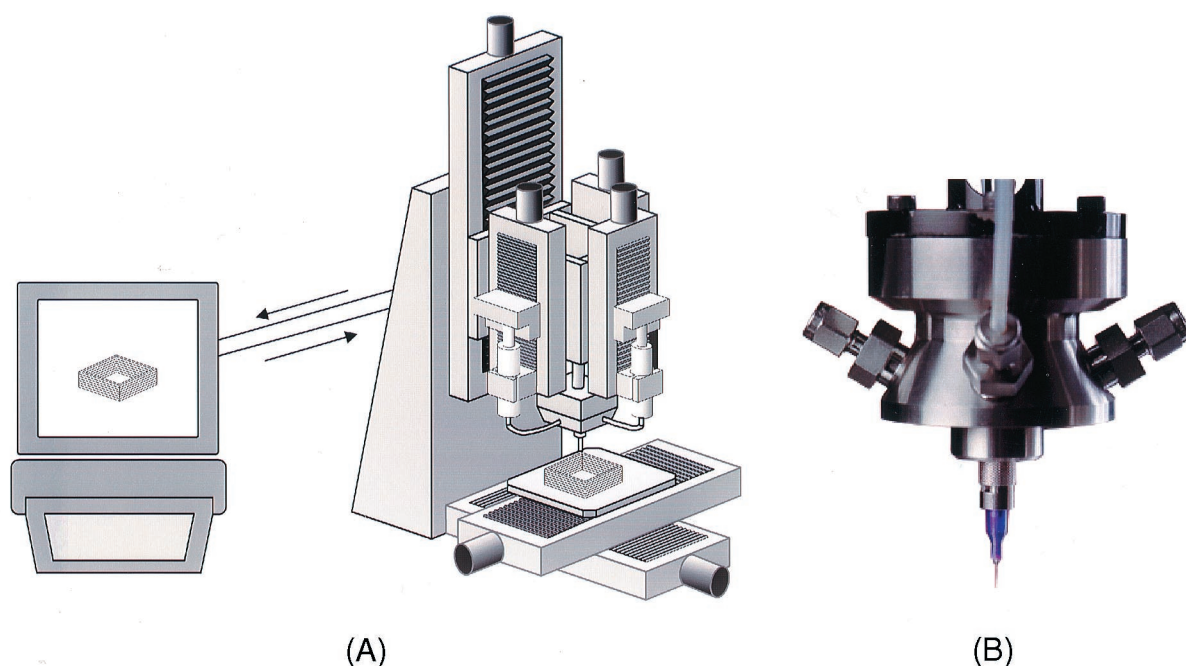


**Fig. A-1.** (A) Schematic illustration of robocasting equipment and (B) optical view of robocasting head, which deposits a concentrated colloidal suspension in a layer-by-layer build sequence to generate complex, three-dimensional parts.

balancing opposing viscous and electric forces:

$$U_e = \frac{\epsilon_r \epsilon_0 \zeta E}{f_H \eta_0} \quad (29)$$

where  $\zeta$  is the zeta-potential,  $E$  the electric field, and  $f_H$  the Henry constant, which is equal to 1 when  $\kappa a > 100$ , and to 1.5 when  $\kappa a < 1$ .<sup>6</sup> This expression is valid for a dilute, stable suspension. A recent review of this forming method is provided by Sarkar and Nicholson.<sup>127</sup>

### (3) Consolidation via Gelation

The formation of a dense, solid layer or body occurs via gelation in several forming routes, including aqueous injection molding (AIM),<sup>129,130</sup> gelcasting,<sup>48–50</sup> and direct coagulation casting (DCC).<sup>46,47</sup> These techniques rely on either physical or chemical

approaches to induce gelation in a concentrated colloidal suspension ( $\phi_{\text{eff}} \geq 0.5$ ). Gelation denotes the transition from a liquid (sol) to a solid (gel) state that occurs in the absence of fluid removal. During this process, discrete species in solution undergo growth (e.g., monomers or linear polymers  $\rightarrow$  polymer network or colloidal particles  $\rightarrow$  aggregated particle network). At the sol–gel transition, dramatic changes in the viscoelastic properties of the system are observed, as shown in Fig. 14.<sup>131</sup> The viscosity of the system increases with time before its divergence to infinity at the gel point, which coincides with the formation of a three-dimensional space-filling cluster whose characteristic size is on the order of the sample dimensions. If growth is arrested because of depletion of reactant before gel formation, the system remains in the liquid state, and its apparent viscosity plateaus to a steady-state value,  $\eta_{\text{equil}}$ . Beyond the gel point, additional linkages form between growing clusters, thereby strengthening the gel network,

## Panel A. Continued

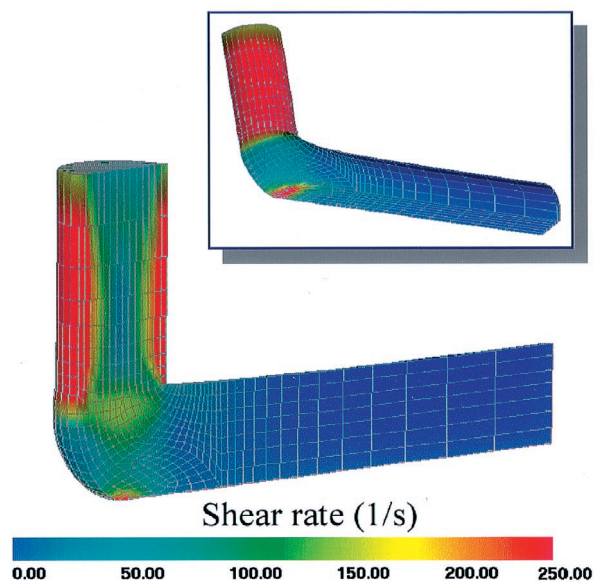


**Fig. A-2.** Calculated shear rate ( $\dot{\gamma}$ ) for representative deposition conditions, where suspension viscosity is 100 Pa·s, tip diameter is 0.254 mm, and table speed is 5 mm/s. (Views shown correspond to bead cross section and outer surface (inset).) (Adapted from Ref. 118.)

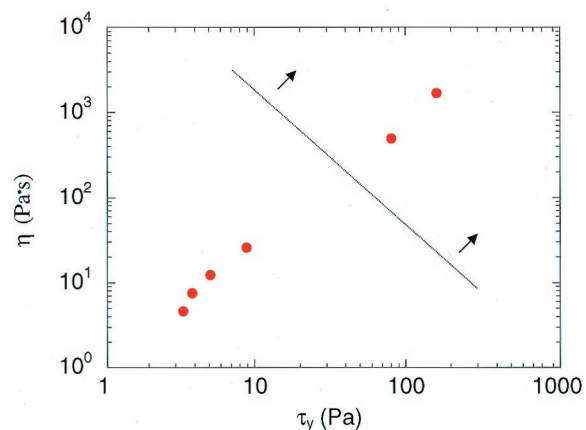
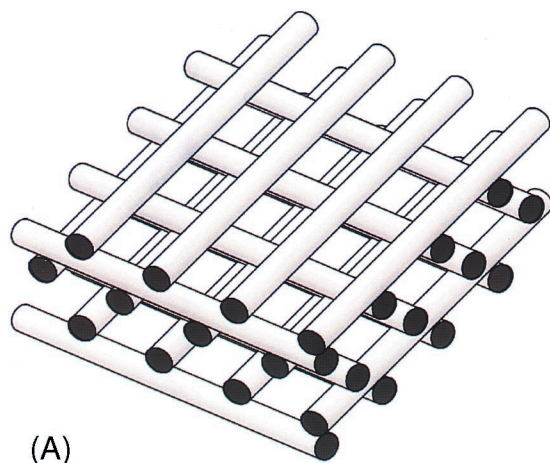
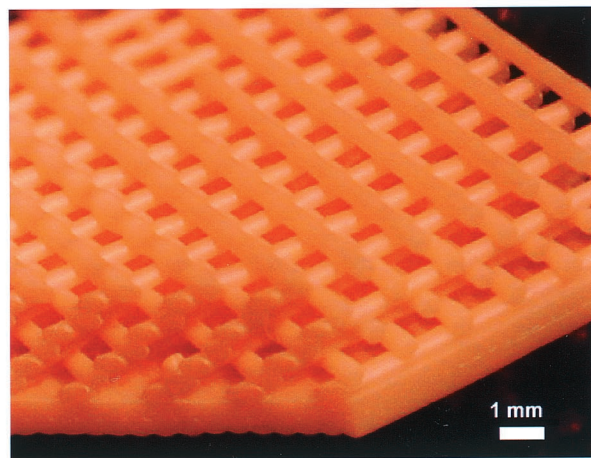


**Fig. A-3.** log-log plot of apparent viscosity (at  $1 \text{ s}^{-1}$ ) as a function of yield stress for aqueous lead zirconate titanate suspensions prepared at 53 vol% solids and varying pH. (Printable conditions for spanning structures correspond to data shown above dashed line.) (Adapted from Ref. 163.)



(A)



(B)

**Fig. A-4.** Periodic lattices for functional ceramic devices: (A) schematic illustration of desired structure and (B) lead zirconate titanate layers deposited via robocasting. (Circular bead cross section is preserved during deposition and drying process.) (Adapted from Ref. 164.)

as reflected by the coincident increase in  $G'$  to a steady-state value  $G'_{\text{equil}}$ .  $G'_{\text{equil}}$  provides a measure of the handling strength or demolding capabilities of the system.

Fanelli *et al.*<sup>130</sup> developed an AIM technique in which a concentrated ceramic suspension is prepared in an agarose-based liquid vehicle. On casting into a chilled mold, the system undergoes temperature-induced physical gelation ( $T_{\text{gel}} \approx 37^\circ\text{C}$ ) because of the change in solvency conditions of the agarose species in solution. The AIM process is compatible with existing commercial injection-molding equipment and yields high-strength components that can be green machined. Unlike conventional IM, however, such components contain relatively low binder content ( $\sim 10$  vol% or less).

Gelcasting, developed by Janney and co-workers,<sup>48,49</sup> uses a concentrated ceramic slurry suspended in a monomeric solution,

which is gelled by *in situ* polymerization. The as-formed organic network encapsulates the ceramic particles, imparting high green strength, which allows for green machining. Recently, Morissette and Lewis<sup>50</sup> developed an alternate gelcasting approach based on polymer cross linking via metal-ion complexation that is amenable for robocasting, as mentioned previously.

Direct coagulation casting (DCC), developed by Gauckler and co-workers,<sup>46,47</sup> relies on physical gelation of colloidal particles, as opposed to organic network formation in AIM and gelcasting. In DCC, electrostatically stabilized, concentrated colloidal suspensions undergo enzyme- or pH-catalyzed reactions to produce  $\text{H}_3\text{O}^+$  or  $\text{OH}^-$  ions or solubilized salt. Such species minimize double-layer repulsive forces by either shifting pH toward the IEP or increasing the ionic strength of the system, resulting in the destabilization illustrated schematically in Fig. 4. The inherent

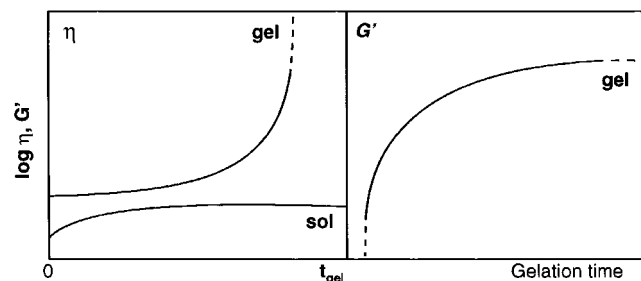


**Fig. 14.** Schematic illustration of rheological property evolution as a function of gelation time for gelling systems, where  $\eta$  is the apparent viscosity and  $G'$  the elastic modulus. (Incomplete gelation leads to a sol phase whose apparent viscosity approaches a steady-state value with time.<sup>131</sup>)

advantages of this approach include minimal binder content ( $\leq 1$  vol%) and homogeneous packing densities. However, the DCC process is limited by long coagulation times and low-strength, as-formed bodies that are not machinable in the green state. Moreover, their high salt content can lead to problems during drying (refer to Section VI) as well as affect component performance. A review of this technique is provided by Gauckler.<sup>47</sup>

## VI. Drying Behavior

Drying is a critical step in colloidal processing of ceramic films and bulk forms. It is a multistage process that involves capillary-driven fluid flow, viscous deformation of the body (or film), evaporation, and diffusion. Removal of the liquid vehicle required for colloidal processing often leads to problems with dimensional control, segregation, and cracking.<sup>3,43,132–141</sup> In recent work, the drying behavior of ceramic layers derived from charge-stabilized colloidal suspensions,<sup>135,136</sup> tape-casting<sup>133,134,137</sup> and gelcasting<sup>142</sup> suspensions, and colloidal suspensions of varying stability<sup>3</sup> has been studied for the purpose of characterizing drying stress and structural evolution.

### (1) Drying Stages

Drying of colloidal assemblies can be divided into three stages: (i) constant-rate period (CRP), (ii) first falling-rate period (FRP1), and (iii) second falling-rate period (FRP2).<sup>141–147</sup> In the CRP, the drying rate is controlled by external conditions. Fluid is supplied via capillary-driven transport to the external surface(s) of the component, where evaporation takes place. As drying proceeds, large pores drain as fluid is drawn to smaller pores with higher suction potential. The drained pores may penetrate far into the component interior, provided the rate of capillary redistribution of fluid exceeds the evaporation rate. Shaw<sup>43</sup> has directly observed the evolution of the liquid–vapor interface during drying of model two-dimensional colloidal layers and has shown that it follows an invasion percolation process.<sup>148</sup> The transition to the FRP1 occurs when fluid can no longer be supplied to the external surface(s) at a rate equivalent to the evaporation rate observed during the CRP. In FRP1, evaporation occurs from the fluid menisci, causing them to retreat into the body (i.e., the funicular state). As further evaporation occurs, fluid resides in isolated pockets (i.e., the pendular state), thereby marking the transition to FRP2. In FRP2, the remaining liquid is removed from the body by vapor-phase diffusion.

### (2) Capillary-Driven Fluid Flow

During drying, the transport of liquid through a porous medium is governed by the pressure gradient resulting from the capillary pressure  $P_{\text{cap}}$ .<sup>138</sup>

$$P_{\text{cap}} = \frac{2\gamma_{\text{LV}}}{r_p} \quad (30)$$

where  $\gamma_{\text{LV}}$  is the liquid–vapor surface tension and  $r_p$  the characteristic pore size, which can be approximated by the hydraulic radius,  $r_h$ .<sup>138</sup>

$$r_h = \frac{2(1 - \phi)}{A_s \phi \rho} \quad (31)$$

In accordance with Darcy's law, the liquid flux ( $J$ ) is proportional to the pressure gradient in the liquid,  $\partial P/\partial x$ :

$$J = -\frac{D}{\eta_0} \frac{\partial P}{\partial x} \quad (32)$$

where  $\eta_0$  is the solution viscosity and  $D$  the permeability given by<sup>149</sup>

$$D = \frac{(1 - \phi)^3}{5(A_s \phi \rho_s)^2} \quad (33)$$

where  $\phi$ ,  $A_s$ , and  $\rho$  have been defined previously. The length scale ( $l_{\text{cap}}$ ) over which capillary migration occurs during drying has been derived previously:<sup>28,136</sup>

$$l_{\text{cap}} = \left[ \frac{2H(\Delta P)(1 - \phi)^3}{5V_E \eta_0 (A_s \phi \rho_s)^2} \right]^{1/2} \quad (34)$$

where  $H$  is the layer thickness,  $V_E$  the evaporation rate, and  $\Delta P$  the pressure drop estimated from Eq (30). The importance of capillary-driven liquid migration is shown by comparing  $l_{\text{cap}}$  to the characteristic size of the drying layer (or body)  $H$ . When  $l_{\text{cap}} > H$ , the liquid–vapor interface penetrates into the layer as an irregular front. In contrast, when  $l_{\text{cap}} \ll H$ , the liquid–vapor interface penetrates into the body as a planar front. This latter situation should be avoided, because it leads to a sharp stress gradient that promotes cracking. As shown in Eq (34),  $l_{\text{cap}}$  can be increased by decreasing the drying rate  $V_E$ , increasing the initial solids loading in suspension, or decreasing the fluid viscosity.

### (3) Drying Stress and Structural Evolution

Stress evolution during drying has been measured *in situ* for ceramic layers prepared from charged stabilized alumina suspensions,<sup>136</sup> tape-casting<sup>137</sup> and gelcasting<sup>142</sup> suspensions, and colloidal silica suspensions of varying stability.<sup>3</sup> Four regions of behavior have been delineated for binder-free layers: (i) stress rise ( $\sigma_{\text{rise}}$ ); (ii) stress maximum ( $\sigma_{\text{max}}$ ); (iii) stress decay ( $\sigma_{\text{decay}}$ ); and (iv) residual stress ( $\sigma_{\text{res}}$ ), as illustrated schematically in Fig. 15. During the initial stress rise period, evaporative processes lead to an increase in colloid volume fraction in the layers. Consolidation persists until the particle network can completely support the

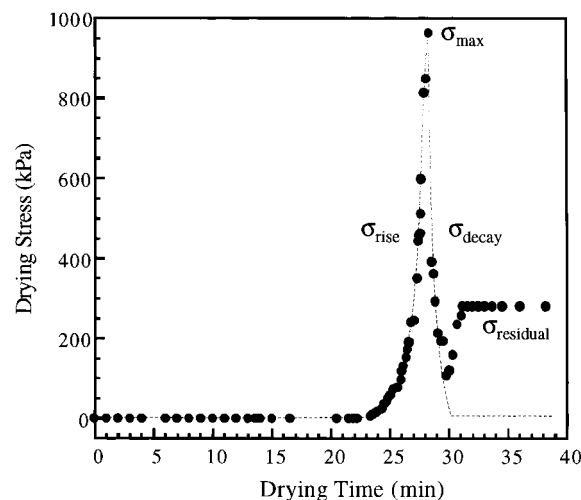


**Fig. 15.** Schematic illustration of the characteristic stress evolution during drying of binder-free, colloidal films cast onto a rigid substrate ((- -) behavior expected in the absence of salt species).

drying stress imposed by capillarity. The average measured stress ( $\sigma_{\text{rise}}$ ) at any given time is related to the compressive stress imposed on the solid particle network ( $\sigma_s$ ) within the film by<sup>132</sup>

$$\sigma_s = \sigma_{\text{rise}} \left( 1 - \frac{1 - \phi}{C_v} \right) \approx \sigma_{\text{rise}} \frac{4\phi - 1}{3} \quad (35)$$

where  $C_v = (1 - 2\nu)/(1 - \nu)$ ; when the Poisson ratio ( $\nu$ ) is 0.2,  $C_v = 3/4$ .

Because no external loads are applied during drying, mechanical equilibrium requires that the capillary tension developed in the fluid phase exert a compressive force of equal magnitude on the particulate network.<sup>92,138</sup> Guo and Lewis<sup>3</sup> recently showed that there is strong correlation between the measured drying stress behavior and the compressive rheological response of the suspended system. For dispersed systems, the stress transmitted between the particles is defined by the osmotic pressure ( $\Pi$ ) which results from repulsive interparticle interactions (refer to Eq. (19)). For flocculated systems, the stress transmitted through a space-filling, aggregated particle network is defined as the compressive yield stress ( $P_y(\phi)$ ; refer to Eq. (24)). During drying of dispersed and flocculated silica layers, Guo and Lewis found excellent agreement between the measured  $\phi$ -dependent  $\sigma_s$  and the respective  $\Pi(\phi)$  and  $P_y(\phi)$  behavior.

Capillary-induced structural rearrangement of the particle network during drying has a profound effect on the final microstructure of the as-dried ceramic layers. The impact of such rearrangement processes is perhaps most readily observed when comparing the extent of consolidation in the absence (i.e., gravity-driven sedimentation) and presence (i.e., drying) of capillarity for the silica films described above (refer to Fig. 16). As expected, films produced from dispersed suspensions yielded higher packing densities than those produced from aggregated suspensions. In both consolidation processes, the packing density exhibited a modest dependence on initial silica volume fraction. The most dramatic increases in film density between gravity- and capillary-driven consolidation were observed for the flocculated systems. For example, the weakly and strongly flocculated systems settled to maximum volume fractions of  $\sim 0.25$  and  $0.15$ , respectively. In contrast, under capillary-driven consolidation, these respective systems achieved maximum volume fractions of  $\sim 0.55$  and  $0.45$ —almost a threefold increase in the latter case. These data indicate that even strongly aggregated particle clusters can be disrupted and packed more efficiently as drying proceeds (i.e., as the compressive stress on the particle network increases because of increased capillary tension in the liquid phase). The important implication of these findings is that, to achieve a high solids loading on drying, one must tailor the compressive flow behavior of the particle network (e.g., its attractive strength) such that the applied drying stress can induce the desired degree of consolidation.

The stress maximum ( $\sigma_{\text{max}}$ ) coincides with the time required for the drying film to reach 100% saturation, i.e., where further network consolidation essentially ceases. Chiu and Cima<sup>136</sup> showed that the maximum drying stress is proportional to the surface tension ( $\gamma_{LV}$ ) of the liquid phase and inversely proportional to the particle size for layers derived from charge-stabilized suspensions. On this basis, they related  $\sigma_{\text{max}}$  to  $P_{\text{cap}}$  at 100% saturation, as given by Eq. (30). The period of stress decay following the observed maximum drying stress occurs when liquid menisci retreat into the film body, i.e., as the degree of saturation decreases below 100%. In the absence of processing aids (e.g., salt or organic species),  $\sigma_{\text{decay}}$  approaches zero as the degree of saturation approaches 0%.

Lewis and co-workers<sup>3,137</sup> have observed more complicated behavior in the presence of processing additives. For example, an additional period of stress rise was observed in silica layers that contained salt species. This observation was attributed to bridging effects resulting from salt precipitation in the final stage of drying. The migration of such species to the external surface of these layers was also evident during drying, leading to severe microstructural nonuniformity.<sup>3</sup> In contrast, the drying stress histories of

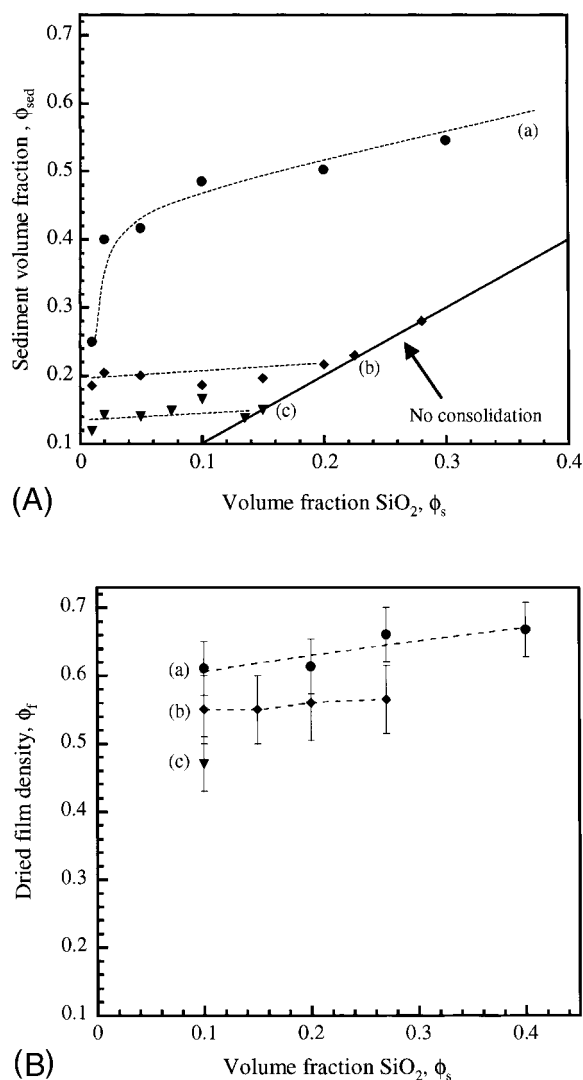


**Fig. 16.** Comparison of (A) sediment volume fraction and (B) dried film volume fraction versus initial solids volume fraction on consolidation of colloidal silica suspensions of varying stability: (a) dispersed; (b) weakly flocculated; and (c) strongly flocculated.

tape-cast<sup>137</sup> and gelcast ceramic layers<sup>142</sup> are dominated by the organic phase in the later stage of drying. For example, polymer relaxation processes (which are aided by plasticizer additions) are important for tape-cast layers.<sup>137,150–152</sup> Preliminary observations of the drying behavior of gelcast layers reveal even more complex behavior because of the simultaneous effects of drying and chemical gelation of the organic species in solution.<sup>142</sup> Because many emerging forming routes rely on gel-based processes, via the formation of either a flocculated particulate network or a colloid-filled, organic gel linked by physical or chemical means, further studies of such systems are warranted.

## VII. Future Directions

This review of colloidal processing of ceramics, combined with related areas of colloid science, suggests certain research directions. The primary motivation for adopting a colloidal-based methodology for ceramics fabrication is to enable control over structural evolution, hence, eliminating unwanted heterogeneities. As described in Sections III–VI, one must tailor interparticle forces, suspension rheology, consolidation, and drying behavior to achieve the optimal microstructure for a given application. The ultimate success of this approach requires fundamental knowledge of the interrelations between the structure of colloidal assemblies and these various properties.

The theoretical understanding of interparticle forces is relatively mature; however, there is a need for direct force measurements in ceramic systems of varying colloid chemistry, crystallographic orientation, adsorbed layer chemistry, and solution composition (e.g., electrolyte species and nonadsorbed polymer or polyelectrolyte species). The advent of new measurement tools, such as atomic force microscopy in colloidal probe mode, has opened up the possibility of conducting such measurements. Although several studies have been reported recently,<sup>24,73,153–157</sup> this remains a wide-open research area. Particular emphasis should be directed toward the interaction between tailored particle interfaces. To adequately investigate such phenomena, *smooth, spherical* colloidal probes of varying composition must be fabricated. This remains a challenge for many ceramic systems of interest. At present, densified, spray-dried granules are commonly utilized. However, the surface roughness associated with these colloidal probes complicates force–distance curve analysis considerably. Once this challenge has been met, direct measurement of interparticle forces between ceramic surfaces with tailored adsorbed layers should be systematically conducted. Specifically, novel adlayer configurations, such as diblock and triblock copolymers of varying segment length and composition (including ionizable groups), should be characterized. The ultimate goal is to provide the knowledge base needed to design functional dispersants that yield the targeted colloidal stability (e.g., tunable barrier height or well depth) required for ceramics processing. Recognizing that such species are often present in solution as well as in the adsorbed state, we are also required to develop a proper understanding of depletion-driven effects.

The rheological behavior of model colloidal suspensions is well understood. However, the ability to predict flow behavior of concentrated suspensions directly from pair potential interactions is lacking. The many-body nature of these interactions in suspension is not well understood. There is a need for more-sophisticated theories, as well as new characterization methods to probe local suspension structure. Scattering measurements have been an effective tool to study order–disorder<sup>98</sup> and particle-clustering transitions<sup>39</sup> in concentrated systems. However, scattering measurements assess only bulk properties. Recently, van Blaaderen and co-workers<sup>158–61</sup> have demonstrated the utility of confocal microscopy as a structural probe for dense colloidal suspensions ( $\phi \rightarrow \phi_{\max}$ ). Using special silica spheres with a fluorescent dye core in an index-matched solvent, they obtained precise local structural information of colloidal glass<sup>160</sup> and crystalline<sup>161</sup> phases. Experimental work that incorporates direct force measurements, characterization of local suspension structure, and suspension rheology is needed to advance our predictive capabilities.

Emerging colloidal-forming routes have focused on producing bulk ceramics via gel- or SFF-based approaches. There is a need to further understand the relation between the viscoelastic properties, handling strength (i.e., demolding), drying behavior, and network strength of assemblies derived from colloidal gels and colloid-filled organic gels. SFF techniques allow for local compositional control as well as intricate component geometries. However, such techniques can be limited by lengthy build sequences and feature resolution ( $\sim 25 \mu\text{m}$  minimum size). There is need to develop controlled methods of rapidly placing suspension volumes approaching  $10 \mu\text{m}^3$  to facilitate surface patterning, thin film, and small-scale component fabrication. The assembly and drying of colloidal systems is expected to become more challenging as the use of nanoparticles increases.

In summary, the field of ceramics processing will not only contribute to, but advance through, discoveries in related areas such as self-assembly of materials, complex fluids, photonic materials, and nanotechnology.

### Acknowledgments

It is a pleasure to acknowledge the many people who have contributed to my knowledge and interest in colloidal processing of ceramics. Specifically, I thank M. J. Cima, W. Rhine, H. K. Bowen, and the students and technicians associated with MIT-CPRL as well as D. Payne, C. Zukoski, K. Schweizer, and my research group at

UIUC. My research group has benefited from fruitful collaborations with J. Cesarano and D. Dimos (Sandia National Laboratories), F. F. Lange (UCSB), J. Walz (Yale), P. Braun (UIUC), and Pierre Wiltzius (Bell Labs/Lucent Technologies). Finally, C. Martinez and J. Smay deserve a special note of gratitude for their assistance with the preparation of this paper.

### References

- F. F. Lange, "Powder Processing Science and Technology for Increased Reliability," *J. Am. Ceram. Soc.*, **72** [1] 3–15 (1989).
- I. A. Aksay, "Microstructure Control through Colloidal Consolidation"; pp. 94–104 in *Advances in Ceramics*, Vol. 9, *Forming of Ceramics*. Edited by J. A. Mangels and G. L. Messing. American Ceramic Society, Columbus, OH, 1984.
- J. Guo and J. A. Lewis, "Aggregation Effects on Compressive Flow Properties and Drying Behavior of Colloidal Silica Suspensions," *J. Am. Ceram. Soc.*, **82** [9] 2345–58 (1999).
- F. H. Norton, *Elements of Ceramics*, 2nd ed.; pp. 1–5. Addison-Wesley, Reading, MA, 1974.
- F. H. Norton, *Fine Ceramics: Technology and Applications*; pp. 8–19. McGraw-Hill, New York, 1970.
- J. S. Reed, *Introduction to the Principles of Ceramic Processing*; pp. 3–15. Wiley, New York, 1988.
- W. D. Kingery, "Firing—The Proof Test for Ceramic Processing"; pp. 291–305 in *Ceramic Processing Before Firing*. Edited by G. Y. Onoda Jr. and L. L. Hench. Wiley, New York, 1978.
- H. K. Bowen, "Basic Research Needs on High-Temperature Ceramics for Energy Applications," *J. Mater. Sci. Eng.*, **44** [1] 1 (1980).
- W. H. Rhodes, "Agglomeration and Particle Size Effects on Sintering of Yttria-Stabilized Zirconia," *J. Am. Ceram. Soc.*, **64**, 19–22 (1981).
- F. F. Lange *et al.*, "Processing Related Fracture Origins: I, II, and III," *J. Am. Ceram. Soc.*, **65**, 396–408 (1983).
- W. Stober, A. Fink, and E. Bohn, "Controlled Growth of Monodisperse Silica Spheres in the Micron Size Range," *J. Colloid Interface Sci.*, **26**, 62–69 (1968).
- E. Matijevic, "Monodispersed Metal (Hydrous) Oxides—A Fascinating Field of Colloid Science," *Acc. Chem. Res.*, **14**, 22–29 (1981).
- E. A. Barringer and H. K. Bowen, "Formation, Packing, and Sintering of Monodisperse  $\text{TiO}_2$  Powders," *J. Am. Ceram. Soc.*, **65** [12] C-199–C-201 (1982).
- Other references can be found in Materials Research Society Symposium Proceedings, Vol. 32, *Better Ceramics Through Chemistry*. Edited by C. J. Brinker, D. E. Clark, and D. R. Ulrich. Elsevier, New York, 1984.
- H. C. Hamaker, "The London–van der Waals Attraction between Spherical Particles," *Physica (Amsterdam)*, **4**, 1058–72 (1937).
- B. V. Derjaguin and L. D. Landau, "Theory of Stability of Highly Charged Lyophobic Sols and Adhesion of Highly Charged Particles in Solutions of Electrolytes," *Acta Physicochim. URSS*, **14**, 633–52 (1941).
- E. J. W. Verwey and J. Th. G. Overbeek, *Theory of Stability of Lyophobic Colloids*. Elsevier, Amsterdam, The Netherlands, 1948.
- R. Evans and D. H. Napper, "Kolloid Steric Stabilization II. A Generalization of Fischer's Solvency Theory," *Kolloid-Z. Polymere*, **251**, 329 (1973).
- S. Asakura and F. Oosawa, "On Interactions between Two Bodies Immersed in a Solution of Macromolecules," *J. Chem. Phys.*, **22**, 1255 (1955).
- S. Asakura and F. Oosawa, "Interactions between Particles Suspended in Solutions of Macromolecules," *J. Polym. Sci.*, **33**, 183 (1958).
- D. Tabor and R. H. S. Winterton, "The Direct Measurement of Normal and Retarded van der Waals Forces," *Proc. R. Soc. London A*, **312**, 435–50 (1969).
- J. N. Israelachvili and D. Tabor, "The Measurement of van der Waals Dispersion Forces in the Range 1.5 to 130 nm," *Proc. R. Soc. London A*, **331** 19–38 (1972).
- J. N. Israelachvili and G. E. Adams, "Measurement of Forces between Two Mica Surfaces in Aqueous Electrolyte Solutions in the Range 0–100 nm," *J. Chem. Soc. Faraday Trans.*, **1**, **74**, 975–1001 (1978).
- W. A. Drucker, T. J. Senden, and R. M. Pashley, "Direct Measurement of Colloidal Forces Using an Atomic Force Microscope," *Langmuir*, **8**, 1831–36 (1992).
- W. E. Worrall, *Clays and Ceramic Raw Materials*; pp. 79–154. Wiley, New York, 1975.
- F. F. Lange, B. I. Davis, and E. Wright, "Processing-Related Fracture Origins: IV, Elimination of Voids Produced by Organic Inclusions," *J. Am. Ceram. Soc.*, **69** [1] 66–69 (1986).
- P. Calvert and M. J. Cima, "Theoretical Models for Binder Burnout," *J. Am. Ceram. Soc.*, **73** [3] 575–79 (1990).
- M. J. Cima, J. A. Lewis, and A. D. Devoe, "Binder Distribution in Ceramic Greenware," *J. Am. Ceram. Soc.*, **72** [7] 1192–99 (1989).
- J. A. Lewis and M. J. Cima, "Diffusivities of Dialkyl Phthalates in Plasticized Poly(vinyl butyral): Impact on Binder Thermolysis," *J. Am. Ceram. Soc.*, **73** [9] 2702–707 (1990).
- I. A. Aksay, "Principles of Ceramic Shape-Forming with Powder Systems"; pp. 663–74 in *Ceramic Transactions*, Vol. 1, *Ceramic Powder Science II (A and B)*. Edited by G. L. Messing, E. R. Fuller, and H. Hausner. American Ceramic Society, Westerville, OH, 1988.
- D. W. Schaefer, J. E. Martin, P. Wiltzius, and D. S. Cannell, "Fractal Geometry of Colloidal Aggregates," *Phys. Rev. Lett.*, **52**, 2371 (1984).
- D. A. Weitz and M. Oliveria, "Fractal Structures Formed by Kinetic Aggregation of Aqueous Gold Colloids," *Phys. Rev. Lett.*, **52** [16] 1433–36 (1984).
- M. Carpineti, F. Ferri, M. Giglio, E. Paganini, and U. Perini, "Salt-Induced Fast Aggregation of Polystyrene Latex," *Phys. Rev. A: Gen. Phys.*, **42** [12] 7347–54 (1990).
- C. Allain, M. Cloitre, and M. Wafra, "Aggregation and Sedimentation in Colloidal Suspensions," *Phys. Rev. Lett.*, **74** [8] 1478–81 (1995).
- G. H. Bogush and C. F. Zukoski IV, "Uniform Silica Particle Precipitation: An Aggregative Growth Model," *J. Colloid Interface Sci.*, **142** [1] 19–34 (1990).

- <sup>36</sup>R. Buscall, P. D. A. Mills, J. W. Goodwin, and D. W. Lawson, "Scaling Behavior of the Rheology of Aggregate Networks Formed from Colloidal Particles," *J. Chem. Soc. Faraday Trans. 1*, **84** [12] 4249–60 (1988).
- <sup>37</sup>B. J. Ackerson, "Shear-Induced Order and Shear Processing of Model Hard-Sphere Suspensions," *J. Rheol. (N.Y.)*, **34** [4] 553–90 (1990).
- <sup>38</sup>L. Marshall and C. F. Zukoski, "Experimental Studies on the Rheology of Hard-Sphere Suspensions Near the Glass Transition," *J. Phys. Chem.*, **94**, 1164–71 (1994).
- <sup>39</sup>J. Bender and N. J. Wagner, "Reversible Shear Thickening in Monodisperse and Bidisperse Colloidal Dispersions," *J. Rheol.*, **40**, 899 (1996).
- <sup>40</sup>J. Guo and J. A. Lewis, "Effects of Ammonium Chloride on the Rheological Properties and Sedimentation Behavior of Colloidal Silica Suspensions," *J. Am. Ceram. Soc.*, **83** [2] 266–72 (2000).
- <sup>41</sup>R. Buscall, "The Sedimentation of Concentrated Colloidal Suspensions," *Colloids Surf.*, **43**, 33–53 (1990).
- <sup>42</sup>T. Okubo, "Sedimentation Velocity of Colloidal Spheres in Deionized Suspension," *J. Phys. Chem.*, **98**, 1472–74 (1994).
- <sup>43</sup>T. M. Shaw, "Drying as an Immiscible Displacement Process with Fluid Counterflow," *Phys. Rev. Lett.*, **59** [15] 1671–74 (1987).
- <sup>44</sup>B. V. Velamakanni, J. C. Chang, F. F. Lange, and D. S. Pearson, "New Method for Efficient Colloidal Particle Packing via Modulation of Repulsive Lubricating Hydration Forces," *Langmuir*, **6** [7] 1323–25 (1990).
- <sup>45</sup>F. F. Lange, "New Interparticle Potential Paradigm for Advanced Powder Processing"; pp. 185–201 in *Ceramic Transactions, Vol. 22, Ceramic Powder Science IV*. Edited by S.-I. Hirano, G. L. Messing, and H. Hausner. American Ceramic Society, Westerville, OH, 1991.
- <sup>46</sup>T. J. Graule, W. Si, F. H. Baader, and L. J. Gaukler, "Direct Coagulation Casting (DCC): Fundamentals of a New Forming Process for Ceramics"; pp. 457–61 in *Ceramic Transactions, Vol. 51, Ceramic Processing Science and Technology*. Edited by H. Hausner, G. L. Messing, and S.-I. Hirano. American Ceramic Society, Westerville, OH, 1995.
- <sup>47</sup>L. J. Gaukler, Th. Graule, and F. Baader, "Ceramic Forming Using Enzyme Catalyzed Reactions," *Mater. Chem. Phys.*, **61**, 78–102 (1999).
- <sup>48</sup>O. O. Omatete, M. A. Janney, and R. A. Strehlow, "Gelcasting—A New Ceramic Forming Process," *Am. Ceram. Soc. Bull.*, **70** [10] 1641–49 (1991).
- <sup>49</sup>A. C. Young, O. O. Omatete, M. A. Janney, and P. A. Menchhofer, "Gelcasting of Alumina," *J. Am. Ceram. Soc.*, **74** [3] 612–18 (1991).
- <sup>50</sup>S. Morissette and J. A. Lewis, "Chemorheology of Aqueous Alumina-Poly(vinyl alcohol) Gelcasting Suspensions," *J. Am. Ceram. Soc.*, **82** [3] 521–28 (1999).
- <sup>51</sup>E. Sachs, M. Cima, and P. Williams, "Three-Dimensional Printing: Rapid Tooling and Prototypes Directly from CAD Model," *J. Eng. Ind.*, **114** [4] 481–88 (1992).
- <sup>52</sup>J. Cesarano, R. Segalman, and P. Calvert, "Robocasting Provides Moldless Fabrication from Slurry Deposition," *Ceram. Ind.*, 94–102 (1998).
- <sup>53</sup>M. L. Griffith and J. W. Halloran, "Freeform Fabrication of Ceramics via Stereolithography," *J. Am. Ceram. Soc.*, **79** [10] 2601–608 (1996).
- <sup>54</sup>J. Cawley, "Computer-Aided Manufacturing of Laminated Engineering Materials (CAM-LEM) and Its Applications to the Fabrication of Ceramic Components without Tooling"; pp. 1–5 in *Proceedings of the 1997 International Gas Turbine and Aeroengine Congress and Exposition*. American Society of Mechanical Engineers, New York, 1997.
- <sup>55</sup>M. Agarwala, A. Bandyopadhyay, R. van Weerwn, et al., "FDC, Rapid Fabrication of Structural Components," *Am. Ceram. Soc. Bull.*, **75** [11] 60–66 (1996).
- <sup>56</sup>R. J. Hunter, *Foundations of Colloid Science*, Vols. 1 and 2; pp. 168–224. Oxford University Press, Oxford, U.K., 1987 and 1989.
- <sup>57</sup>R. H. French, "Origins and Applications of London Dispersion Forces and Hamaker Constants in Ceramics," *J. Am. Ceram. Soc.*, **83** [9] 2117 (2000).
- <sup>58</sup>D. B. Hough and L. R. White, "The Calculation of Hamaker Constants from Lifshitz Theory with Applications to Wetting Phenomena," *Adv. Colloid Interface Sci.*, **14**, 3–14 (1980).
- <sup>59</sup>H. D. Ackler, R. H. French, and Y.-M. Chiang, "Comparisons of Hamaker Constants for Ceramic Systems with Intervening Vacuum or Water: From Force Laws and Physical Properties," *J. Colloid Interface Sci.*, **179**, 460–69 (1996).
- <sup>60</sup>L. Bergström, A. Meurk, H. Arwin, and D. J. Rowcliffe, "Estimation of Hamaker Constants for Ceramic Materials from Optical Data Using Lifshitz Theory," *J. Am. Ceram. Soc.*, **79** [2] 339–48 (1996).
- <sup>61</sup>L. Bergström, "Hamaker Constants of Inorganic Materials," *Adv. Colloid Interface Sci.*, **70**, 125–69 (1997).
- <sup>62</sup>J. N. Israelachvili, *Intermolecular and Surface Forces*; p. 246. Academic Press, New York, 1992.
- <sup>63</sup>A. L. Ogden and J. A. Lewis, "Effect of Nonadsorbed Polymer on the Stability of Weakly Flocculated Nonaqueous Suspensions," *Langmuir*, **12** [14] 3413–24 (1996).
- <sup>64</sup>D. A. R. Jones, B. Leary, and D. V. Boger, "The Rheology of a Concentrated Colloidal Suspension of Hard Spheres," *J. Colloid Interface Sci.*, **147**, 479 (1991).
- <sup>65</sup>H. de Hek and A. Vrij, "Interactions in Mixtures of Colloidal Silica Spheres and Polystyrene Molecules in Cyclohexane," *J. Colloid Interface Sci.*, **84**, 409 (1981).
- <sup>66</sup>W. J. Frith, T. A. Strivens, and W. B. Russel, "The Rheology of Suspensions Containing Polymerically Stabilized Particles," *J. Colloid Interface Sci.*, **139**, 55 (1990).
- <sup>67</sup>J. C. Chang, F. F. Lange, D. S. Pearson, and J. P. Pollinger, "Pressure Sensitivity for Particle Packing of Aqueous Al<sub>2</sub>O<sub>3</sub> Slurries vs Interparticle Potential," *J. Am. Ceram. Soc.*, **77** [5] 1357–60 (1994).
- <sup>68</sup>D. H. Napper, *Polymeric Stabilization of Colloidal Dispersions*; pp. 4–13. Academic Press, London, U.K., 1983.
- <sup>69</sup>B. Vincent, J. Edwards, S. Emmett, and A. Jones, "Depletion Flocculation in Dispersions of Sterically Stabilized Particles ("Soft Spheres")," *Colloids Surf.*, **18**, 261 (1986).
- <sup>70</sup>N. M. Wara, L. F. Francis, and B. V. Velamakanni, "Addition of Alumina to Celluloseacetate Membranes," *J. Membr. Sci.*, **104**, 43–49 (1995).
- <sup>71</sup>L. Bergström and E. Sjöström, "Temperature-Induced Gelation of Concentrated Ceramic Suspensions," *J. Eur. Ceram. Soc.*, **19**, 2117–23 (1999).
- <sup>72</sup>J. Cesarano III, I. A. Aksay, and A. Bleier, "Stability of Aqueous  $\alpha$ -Al<sub>2</sub>O<sub>3</sub> Suspensions with Poly(methacrylic acid) Polyelectrolyte," *J. Am. Ceram. Soc.*, **71** [4] 250–55 (1988).
- <sup>73</sup>S. Biggs and T. W. Healy, "Electrosteric Stabilization of Colloidal Zirconia with Low Molecular Weight Polyacrylic Acid," *J. Chem. Soc. Faraday Trans.*, **90** [22] 3415–21 (1994).
- <sup>74</sup>D. J. Rojas, P. M. Claesson, D. Muller, and R. D. Neuman, "The Effect of Salt Concentration on Adsorption of Low-Charge-Density Polyelectrolytes and Interactions between Polyelectrolyte-Coated Surfaces," *J. Colloid Interface Sci.*, **205**, 77–78 (1998).
- <sup>75</sup>J. Marra and M. L. Hair, "Forces between Two Poly(2-vinyl pyridine)-Covered Surfaces as a Function of Ionic Strength and Polymer Charge," *J. Phys. Chem.*, **92**, 6044–51 (1988).
- <sup>76</sup>V. Hackley, "Colloidal Processing of Si<sub>3</sub>N<sub>4</sub> with PAA: I, Adsorption and Electrostatic Interactions," *J. Am. Ceram. Soc.*, **80** [9] 2315–25 (1997).
- <sup>77</sup>J. Blaakmeer, M. R. Bohmer, M. A. Cohen Stuart, and G. J. Fleer, "Adsorption of Weak Polyelectrolytes on Highly Charged Surfaces: Poly(acrylic acid) on Polystyrene Latex with Strong Cationic Groups," *Macromolecules*, **23**, 2301–309 (1990).
- <sup>78</sup>M. R. Bohmer, O. A. Evers, and J. M. H. M. Scheutjens, "Weak Polyelectrolytes between Two Surfaces: Adsorption and Stabilization," *Macromolecules*, **23**, 2288–301 (1990).
- <sup>79</sup>J. M. Berg, P. M. Claesson, and R. D. Neuman, "Interactions between Mica Surfaces in Na-PAA Solutions Containing Ca<sup>2+</sup> Ions," *J. Colloid Interface Sci.*, **161**, 182–89 (1993).
- <sup>80</sup>V. Shubin and P. Linse, "Effect of Electrolytes on Adsorption of Cationic Polyacrylimide on Silica: Ellipsometric Study and Theoretical Modeling," *J. Phys. Chem.*, **99**, 1285–91 (1995).
- <sup>81</sup>J. Y. Walz and A. Sharma, "Effect of Long-Range Interactions on the Depletion Force Between Colloidal Particles," *J. Colloid Interface Sci.*, **168**, 485 (1994).
- <sup>82</sup>Y. Mao, M. E. Cates, and H. N. W. Lekkerkerker, "Depletion Forces in Polydisperse Systems," *Physica A*, **222**, 10–24 (1995).
- <sup>83</sup>P. Richetti and P. Kekicheff, "Direct Measurement of Depletion and Structural Forces in a Micellar System," *Phys. Rev. Lett.*, **68**, 1951 (1992).
- <sup>84</sup>J. Israelachvili, "Solvation Forces and Liquid Structure, As Probed by Direct Force Measurements," *Acc. Chem. Res.*, **20**, 415–21 (1987).
- <sup>85</sup>H. K. Christenson, "Interactions between Hydrocarbon Surfaces in a Nonpolar Liquid: Effect of Surface Properties on Solvation Forces," *J. Phys. Chem.*, **90**, 4–6 (1990).
- <sup>86</sup>R. G. Horn, "Surface Forces and Their Action in Ceramic Materials," *J. Am. Ceram. Soc.*, **73** [5] 1117–35 (1990).
- <sup>87</sup>J. Clarke and B. Vincent, "Stability of Nonaqueous Microgel Dispersions in the Presence of Free Polymers," *J. Chem. Soc. Faraday Trans. 1*, **77**, 1831 (1981).
- <sup>88</sup>P. A. Reynolds and C. A. Reid, "Effect of Nonadsorbing Polymers on the Rheology of a Concentrated Non-Aqueous Dispersion," *Langmuir*, **7**, 89 (1991).
- <sup>89</sup>L. Bergström, "Rheology of Concentrated Suspensions"; pp. 193–239 in *Surface and Colloid Chemistry in Advanced Ceramic Processing*. Edited by R. J. Pugh and L. Bergström. Marcel Dekker, New York, 1994.
- <sup>90</sup>W. B. Russell, "Concentrated Colloidal Dispersions," *MRS Bull.*, **16** [8] 27–31 (1991).
- <sup>91</sup>R. Buscall, "Elastic Properties of Structured Dispersions: A Simple Centrifuge Method of Examination," *Colloids Surf.*, **5** [4] 269–83 (1982).
- <sup>92</sup>K. T. Miller, R. M. Melant, and C. F. Zukoski, "Comparison of the Compressive Yield Response of Aggregated Suspensions: Pressure Filtration, Centrifugation, and Osmotic Consolidation," *J. Am. Ceram. Soc.*, **79** [10] 2545–56 (1996).
- <sup>93</sup>R. Buscall and L. White, "The Consolidation of Concentrated Suspensions, Part I—The Theory of Sedimentation," *J. Chem. Soc. Faraday Trans. 1*, **83**, 873–91 (1987).
- <sup>94</sup>W. Shih, W. Y. Shih, S. Kim, and I. Aksay, "Equilibrium-State Density Profiles of Centrifuged Cakes," *J. Am. Ceram. Soc.*, **77** [2] 540–46 (1994).
- <sup>95</sup>I. M. Krieger, "Rheology of Monodisperse Latices," *Adv. Colloid Interface Sci.*, **3**, 111 (1972).
- <sup>96</sup>L. V. Woodcock, "Origins of Shear Dilatancy and Shear Thickening Phenomena," *Chem. Phys. Lett.*, **111**, 455 (1984).
- <sup>97</sup>H. A. Barnes, "Shear Thickening (Dilatancy) in Suspensions of Nonaggregating Solid Particles Dispersed in Newtonian Liquids," *J. Rheol.*, **33**, 329 (1989).
- <sup>98</sup>R. L. Hoffman, "Discontinuous and Dilatant Viscosity Behavior in Concentrated Suspensions. I. Observation of Flow Stability," *Trans. Soc. Rheol.*, **16**, 155 (1972).
- <sup>99</sup>W. J. Frith, T. A. Strivens, and J. Mewis, "Dynamic Mechanical Properties of Polymerically Stabilized Dispersions," *J. Colloid Interface Sci.*, **139**, 55 (1990).
- <sup>100</sup>J. Chapel, "History-Dependent Hydration Forces Measured between Silica Surfaces," *J. Colloid Interface Sci.*, **162**, 517–19 (1994).
- <sup>101</sup>R. Buscall, I. J. McGowan, P. D. A. Mills, R. F. Stewart, D. Sutton, L. R. White, and G. E. Yates, "The Rheology of Strongly Flocculated Suspensions," *J. Non-Newtonian Fluid Mech.*, **24**, 183 (1987).
- <sup>102</sup>K. A. Landman and L. R. White, "Solid/Liquid Separation of Flocculated Suspensions," *Adv. Colloid Interface Sci.*, **51**, 175–246 (1994).
- <sup>103</sup>G. M. Channel and C. F. Zukoski, "Shear and Compressive Rheology of Aggregated Alumina Suspensions," *AIChE J.*, **43** [7] 1700–708 (1997).
- <sup>104</sup>F. F. Lange and K. T. Miller, "Pressure Filtration: Kinetics and Mechanics," *Am. Ceram. Soc. Bull.*, **66** [10] 1498–504 (1987).
- <sup>105</sup>T. J. Fennelly and J. S. Reed, "Mechanics of Pressure Casting," *J. Am. Ceram. Soc.*, **55** [5] 264–68 (1972).
- <sup>106</sup>D. S. Adcock and I. C. McDowall, "The Mechanism of Filter Pressing and Slip Casting," *J. Am. Ceram. Soc.*, **40** [10] 355–60 (1957).

- <sup>107</sup>R. R. Rowlands, "A Review of the Slip Casting Process," *Am. Ceram. Soc. Bull.*, **45** [1] 16–19 (1966).
- <sup>108</sup>I. A. Aksay and C. H. Schilling, "Mechanics of Colloidal Filtration"; see Ref. 2, pp. 85–93.
- <sup>109</sup>K. T. Miller and C. F. Zukoski, "Osmotic Consolidation of Suspensions and Gels," *J. Am. Ceram. Soc.*, **77** [9] 2473–78 (1994).
- <sup>110</sup>G. N. Howatt, R. G. Breckenridge, and J. M. Brownlow, "Fabrication of Thin Sheets for Capacitors," *J. Am. Ceram. Soc.*, **30** [8] 237–420 (1947).
- <sup>111</sup>D. J. Shanefield and R. E. Mistler, "Fine-Grained Alumina Substrates: I. The Manufacturing Process," *Am. Ceram. Soc. Bull.*, **53** [5] 416–20 (1974).
- <sup>112</sup>R. E. Mistler, "Tape Casting: The Basic Process for Meeting the Needs of the Electronic Industry," *Am. Ceram. Soc. Bull.*, **69** [6] 1022–26 (1990).
- <sup>113</sup>L. Bergström, C. H. Schilling, and I. A. Aksay, "Consolidation Behavior of Flocculated Alumina Suspensions," *J. Am. Ceram. Soc.*, **75** [12] 3305–14 (1992).
- <sup>114</sup>Y. T. Chuo, Y. T. Ko, and M. F. Yan, "Fluid Flow Model for Ceramic Tape Casting," *J. Am. Ceram. Soc.*, **70** [10] C-280–C-282 (1987).
- <sup>115</sup>R. Pitchumani and V. M. Karbhari, "Generalized Fluid Flow Model for Ceramic Tape Casting," *J. Am. Ceram. Soc.*, **78** [9] 2497–503 (1995).
- <sup>116</sup>W. Young, "Multilayer Ceramic Technology"; pp. 403–22 in *Ceramic Materials for Electronics*. Edited by R. Buchanan. Marcel Dekker, New York, 1986.
- <sup>117</sup>R. R. Tummala, "Ceramic Packaging"; pp. 455–521 in *Microelectronics Packaging Handbook*. Edited by R. R. Tummala and E. J. Rymaszewski. Van Nostrand Reinhold, New York, 1989.
- <sup>118</sup>S. L. Morissette, J. A. Lewis, J. Cesarano, D. Dimos, and T. Baer, "Solid Freeform Fabrication of Aqueous Alumina–Poly(vinyl alcohol) Gelcasting Suspensions," *J. Am. Ceram. Soc.*, in press.
- <sup>119</sup>G. K. Batchelor, "Sedimentation in a Dilute Dispersion of Spheres," *J. Fluid Mech.*, **52** [2] 245–68 (1972).
- <sup>120</sup>A. P. Philipse, B. C. Bonekamp, and H. J. Veringa, "Colloidal Filtration and (Simultaneous) Sedimentation of Alumina and Silica Suspensions: Influence of Aggregates," *J. Am. Ceram. Soc.*, **73** [9] 2720–27 (1990).
- <sup>121</sup>J. F. Richardson and W. N. Zaki, "The Sedimentation of a Suspension of Uniform Spheres Under Conditions of Viscous Flow," *Chem. Eng. Sci.*, **8**, 65–78 (1954).
- <sup>122</sup>F. F. Lange, "Forming a Ceramic by Flocculation and Centrifugal Casting," U.S. Pat. No. 4 624 808, 1986.
- <sup>123</sup>E. Beylier, R. L. Pober, and M. J. Cima, "Centrifugal Casting of Ceramic Components"; pp. 529–36 in *Ceramic Transactions*, Vol. 12, *Ceramic Powder Science III*. Edited by G. L. Messing, S. Hirano, and H. Hausner. American Ceramic Society, Westerville, OH, 1990.
- <sup>124</sup>J. C. Chang, F. F. Lange, and D. S. Pearson, "Centrifugal Consolidation of Al<sub>2</sub>O<sub>3</sub> and Al<sub>2</sub>O<sub>3</sub>/ZrO<sub>2</sub> Composite Slurries vs Interparticle Potentials: Particle Packing and Mass Segregation," *J. Am. Ceram. Soc.*, **74** [9] 2201–204 (1991).
- <sup>125</sup>P. Sarkar, X. Huang, and P. S. Nicholson, "Structural Ceramic Microlaminates by Electrophoretic Deposition," *J. Am. Ceram. Soc.*, **75**, 2907–909 (1992).
- <sup>126</sup>P. Sarkar, X. Huang, and P. S. Nicholson, "Zirconia/Alumina Functionally Graded Composites by Electrophoretic Deposition," *J. Am. Ceram. Soc.*, **76**, 1055–56 (1993).
- <sup>127</sup>P. Sarkar and P. S. Nicholson, "Electrophoretic Deposition (EPD): Mechanisms, Kinetics, and Application to Ceramics," *J. Am. Ceram. Soc.*, **79** [8] 1987–2002 (1996).
- <sup>128</sup>M. E. Fagan and C. F. Zukoski, "The Rheology of Charge-Stabilized Silica Suspensions," *J. Rheol.*, **41** [2] 373–97 (1997).
- <sup>129</sup>R. D. Rivers, "Method of Injection Molding Powder Metal Parts," U.S. Pat. No. 41 134 180, 1978.
- <sup>130</sup>A. J. Fanelli, R. D. Silvers, W. S., Frei, *et al.*, "New Aqueous Injection Molding Process for Ceramic Powders," *J. Am. Ceram. Soc.*, **72** [10] 1833–36 (1989).
- <sup>131</sup>H. H. Winter, "Polymeric Gels, Materials that Combine Liquid and Solid Properties," *MRS Bull.*, **16** [8] 44–48 (1991).
- <sup>132</sup>G. W. Scherer, "Drying Gels, VIII. Revision and Review," *J. Non-Cryst. Solids*, **109**, 171–82 (1991).
- <sup>133</sup>M. Descamps, M. Mascart, and B. Thierry, "How to Control Cracking of Tape-Cast Sheets," *Am. Ceram. Soc. Bull.*, **74** [3] 89–92 (1995).
- <sup>134</sup>E. Streicher and T. Chartier, "Study of Cracking and Microstructural Evolution during Drying of Tape-Cast Aluminum Nitride Sheets," *J. Mater. Sci.*, **26**, 1659–65 (1991).
- <sup>135</sup>R. C. Chiu and M. J. Cima, "Drying of Granular Ceramic Films: I, Effects of Process Variables on Cracking Behavior," *J. Am. Ceram. Soc.*, **76** [9] 2257–64 (1993).
- <sup>136</sup>R. C. Chiu and M. J. Cima, "Drying of Granular Ceramic Films: II, Drying Stress and Saturation Uniformity," *J. Am. Ceram. Soc.*, **76** [11] 2769–77 (1993).
- <sup>137</sup>J. A. Lewis, K. A. Blackman, A. L. Ogden, J. A. Payne, and L. F. Francis, "Rheological Properties and Stress Development during Drying of Tape-Cast Ceramic Layers," *J. Am. Ceram. Soc.*, **79** [12] 3225–34 (1993).
- <sup>138</sup>D. M. Smith, G. W. Scherer, and J. M. Anderson, "Shrinkage during Drying of Silica Gel," *J. Non-Cryst. Solids*, **188**, 191–206 (1995).
- <sup>139</sup>G. W. Scherer, "Fundamentals of Drying and Shrinkage"; pp. 199–211 in *Science of Whitewares*. Edited by V. E. Henkes, G. Y. Onoda, and W. M. Carty. American Ceramic Society, Westerville, OH, 1997.
- <sup>140</sup>R. D. Deegan, O. Bakajin, T. F. Dupont, G. Huber, S. R. Nagel, and T. A. Witten, "Capillary Flow as the Cause of Ring Stains from Dried Liquid Drops," *Nature (London)*, **389**, 827–29 (1997).
- <sup>141</sup>P. C. Hidber, T. J. Graule, and L. J. Gauckler, "Competitive Adsorption of Citric Acid and Poly(vinyl alcohol) onto Alumina and Its Influence on the Binder Migration during Drying," *J. Am. Ceram. Soc.*, **78** [7] 1775–80 (1995).
- <sup>142</sup>M. A. Huha and J. A. Lewis, "Effects of Polymer Properties on the Chemorheological and Drying Behavior of Alumina–Poly(vinyl alcohol) Gelcasting Suspensions," *J. Am. Ceram. Soc.*, **83** [8] 1957–63 (2000).
- <sup>143</sup>W. B. Haines, "Studies in the Physical Properties of Soils, IV. A Further Contribution to the Theory of Capillary Phenomena in Soil," *J. Agric. Sci.*, **17**, 264 (1927).
- <sup>144</sup>E. W. Comings and T. K. Sherwood, "The Drying of Solids," *Ind. Eng. Chem.*, **26**, 1096–98 (1934).
- <sup>145</sup>N. H. Ceaglske and O. A. Hougen, "The Drying of Granular Solids," *Trans. Am. Inst. Chem. Eng.*, **33**, 283–314 (1937).
- <sup>146</sup>V. H. Scott and A. T. Corey, "Pressure Distribution During Steady Flow in Unsaturated Sands," *Soil Sci. Soc. Am. Proc.*, **25**, 270–74 (1961).
- <sup>147</sup>A. T. Corey and R. H. Brooks, "Drainage Characteristics of Soils," *Soil Sci. Soc. Am. Proc.*, **39**, 211–39 (1975).
- <sup>148</sup>D. Wilkinson and J. F. Willemsen, "Invasion Percolation: A New Form of Percolation Theory," *J. Phys. A: Math. Gen.*, **16**, 3365–76 (1983).
- <sup>149</sup>G. W. Scherer, "Physics of Drying"; pp. 179–97 in *Ultrastructure Processing of Advanced Materials*. Edited by D. R. Uhlmann and D. R. Ulrich. Wiley, New York, 1992.
- <sup>150</sup>L. C. E. Struik, "The Mechanical and Physical Ageing of Semicrystalline Polymers: 1," *Polymer*, **28**, 1521–33 (1987).
- <sup>151</sup>L. C. E. Struik, "The Mechanical and Physical Ageing of Semicrystalline Polymers: 2," *Polymer*, **28**, 1534–42 (1987).
- <sup>152</sup>S. G. Croll, "Internal Strain in Solvent-Cast Coatings," *J. Coat. Technol.*, **51** [648] 64–68 (1979).
- <sup>153</sup>I. Larson, C. J. Drummond, D. Y. C. Chan, and F. Grieser, "Direct Force Measurements between TiO<sub>2</sub> Surfaces," *J. Am. Chem. Soc.*, **115**, 11885–90 (1993).
- <sup>154</sup>A. Milling, P. Mulvaney, and I. Larson, "Direct Measurement of Repulsive van der Waals Interactions Using Atomic Force Microscopy," *J. Colloid Interface Sci.*, **180**, 460–65 (1996).
- <sup>155</sup>A. Milling and S. Biggs, "Direct Measurement of the Depletion Force Using an Atomic Force Microscope," *J. Colloid Interface Sci.*, **170**, 604–606 (1995).
- <sup>156</sup>B. V. Zhmud, A. Meurk, and L. Bergström, "Evaluation of Surface Ionization Parameters from AFM Data," *J. Colloid Interface Sci.*, **1207**, 332–43 (1998).
- <sup>157</sup>J. Sindel, N. Bell, and W. M. Sigmund, "Electrolyte Effects on Nonionic Steric Layers: Bis-hydrophilic PMAA-PEO Diblock Copolymers Adsorbed on Barium Titanate," *J. Am. Ceram. Soc.*, **82** [11] 2953–57 (1999).
- <sup>158</sup>A. van Blaaderen and A. Vrij, "Synthesis and Characterization of Colloidal Dispersions of Fluorescent, Monodisperse Silica Spheres," *Langmuir*, **8**, 2921–31 (1992).
- <sup>159</sup>A. van Blaaderen, A. Imhof, W. Hage, and A. Vrij, "Three-Dimensional Imaging of Submicrometer Colloidal Particles in Concentrated Suspensions Using Confocal Scanning Laser Microscopy," *Langmuir*, **8**, 1514–17 (1992).
- <sup>160</sup>A. van Blaaderen and P. Wiltzius, "Real-Space Structure of Colloidal Hard-Sphere Glasses," *Science (Washington, DC)*, **270**, 1177–79 (1995).
- <sup>161</sup>A. van Blaaderen, R. Ruel, and P. Wiltzius, "Template-Directed Colloidal Crystallization," *Nature (London)*, **385**, 321–24 (1997).
- <sup>162</sup>J. Cesarano and P. Calvert, "Freeforming Objects with Low-Binder Slurry," U.S. Pat. No. 6 027 326, Feb. 22, 2000.
- <sup>163</sup>J. E. Smay, J. A. Lewis, and J. Cesarano, "Viscoelastic Behavior of Weakly Flocculated Lead Zirconate Titanate Suspensions," unpublished work.
- <sup>164</sup>J. E. Smay, J. A. Lewis, and J. Cesarano, "Three-Dimensional Periodic Structures via Robotically Controlled Deposition of Weakly Flocculated Lead Zirconate Titanate Suspensions," unpublished work.
- <sup>165</sup>G. A. Parks, "The Isoelectric Points of Solid Oxides, Solid Hydroxides, and Aqueous Hydroxo Complex Systems," *Chem. Rev.*, **65** [2] 177–98 (1965). □



Jennifer A. Lewis joined the faculty of the Materials Science and Engineering Department at the University of Illinois at Urbana-Champaign in December 1990 after earning her Sc.D. in ceramics science from Massachusetts Institute of Technology. Her research emphasizes fundamental aspects of phase behavior in colloidal systems (e.g., colloid-polymer and colloid-colloid) as well as rheology, assembly, and drying of complex fluids. Dr. Lewis' work in these areas has been recognized internationally by numerous invited lectures, including Gordon Conferences in two separate fields of study. She has received several awards, including NSF Presidential Faculty Fellow Award, Faculty Research Awards from Schlumberger and Allied Signal Foundations, Xerox Junior Faculty Award, and Burnett Teaching Award. Dr. Lewis' experience with The American Ceramic Society includes serving as Associate Editor for the *Journal*, coorganizer of a symposium on colloidal processing, and President of the Ceramics Education Council. Dr. Lewis has published more than 40 invited and peer-reviewed publications.